Atomistic Insights into the Effects of Electromagnetic Fields on an Amyloidogenic Peptide

A thesis submitted in fulfilment of the requirements for the degree of Master of Engineering

Alan Bentvelzen

B. Forensic Sc Hons. Deakin University

School of Engineering

College of Science, Engineering and Health

RMIT University

October 2018

Declaration of Candidature

I certify that except where due acknowledgement has been made, the work is that of the author alone; the work has not been submitted previously, in whole or in part, to qualify for any other academic award; the content of the thesis is the result of work which has been carried out since the official commencement date of the approved research program; any editorial work, paid or unpaid, carried out by a third party is acknowledged; and, ethics procedures and guidelines have been followed.

I acknowledge the support I have received for my research through the provision of an Australian Government Research Training Program Scholarship.

Alan Bentvelzen
15/5/2018

Acknowledgements

This project would not have been possible without the support, guidance, and contribution of many people who deserve to be acknowledged.

I wish to thank my supervisor, Prof. Irene Yarovsky, for giving me the chance to work on this project. Her guidance and assistance have been invaluable throughout the years, and has made my time studying at RMIT very enjoyable.

I would also like to thank my other supervisor, Dr. Nevena Todorova. Thank you so much for all your help, support, and guidance throughout my research project. Your knowledge and experience helped to guide my work to the level of quality it needed.

Acknowledgments to Australian Center of Research Excellence for Electromagnetic Bioeffects Research (ACEBR) for providing financial support on this project.

For providing all the computational facilities, I would like to acknowledge the National Computing Infrastructure (NCI) and the Victorian Partnership for Advanced Computing (VPAC), and Melbourne Bioinformatics.

I would like to acknowledge the rest of the Materials Modelling and Simulations Group. Thank you for making the project not only a productive time, but an enjoyable time as well.

On a personal note, I would like to thank my friends for their support and encouragement over the past few years, with special thanks to Lauren for being the best there ever was, and always being there with wise words when needed.

I would like to thank my partners, Finn and Nic, for their love and support over these years, especially so through the past several months.

Finally, I would like to thank and dedicate this thesis to my parents. Their love and support has allowed me to do a great many things, and ultimately this thesis would not exist without their constant love and support. Thank you so much for everything. I love you.

Table of Contents

Publication List

[1] N. Todorova, **A. Bentvelzen**, N. J. English, I. Yarovsky
"Electromagnetic-field effects on structure and dynamics of amyloidogenic peptides"
Journal of Chemical Physics, Vol. 144, 085101 (2016);
https://doi.org/10.1063/1.4941108

[2] S. P. Loughran, M. S. Al Hossain, **A. Bentvelzen,** … R. J. Croft,
"Bioelectromagnetics Research within an Australian Context: The Australian Centre for Electromagnetic Bioeffects Research (ACEBR)."
International Journal of Environmental Research and Public Health, *13*(10), 967. (2016).
http://doi.org/10.3390/ijerph13100967

[3] **A. Bentvelzen**, N. Todorova, I. Yarovsky
"Conformational response of an amyloidogenic peptide to oscillating electromagnetic fields: Effects of the field frequency and strength" (in progress)

Posters

[1] **A. Bentvelzen***, N. Todorova, I. Yarovsky
"Effects of Electromagnetic Fields on Biological Matter: A Threat or a Treat for Living Organisms?" *Nanotechnology and Medicine Symposium of Tomorrow*, Melbourne, Australia, 2014.

[2] **A. Bentvelzen***, N. Todorova, I. Yarovsky
"Effects of Electromagnetic Fields on Biological Matter: A Threat or a Treat for Living Organisms?" *Ian Snook Conference on Chemical Physics*, Melbourne, Australia, 2014.

[3] **A. Bentvelzen***, N. Todorova, I. Yarovsky
"Modelling EM Field Effects on Protein Structure: Threat or Treat to Human Health?" *Science and Wireless*, Melbourne, Australia, 2015.

[4] N. Todorova, **A. Bentvelzen***, H. Rashid, I. Yarovsky
"Electromagnetic Fields, Proteins and Cell Membranes", *Science and Wireless*, Melbourne, Australia, 2016.

[5] N. Todorova, **A. Bentvelzen***, H. Rashid, I. Yarovsky
"Electromagnetic Fields, Proteins and Cell Membranes", *Beyond Research*, Melbourne, Australia, 2017.

*Presenter

List of Tables

List of Figures

List of Acronyms

Aβ……..Amyloid Beta
AD……..……Alzheimer's Disease
ApoC-II……Apolipoprotein C-II
DNA……..…..Deoxyribonucleic Acid
EM……..Electromagnetic
FF……...……Force Field
GROMACS……..….GROningen Machine for Chemical Simulation
HEWL……...……Hen Egg White Lysozyme
MD……..Molecular Dynamics
NEMD……..…..Non-Equilibrium Molecular Dynamics
NPT…….……Constant Number of particles, pressure and temperature
NVE…….…… Constant Number of particles, volume and temperature
PBC…….…….Periodic Boundary Conditions
PDB……..…Protein Data Bank
RDF……...…….Radial Distribution Function
RF……..Radio Frequency
RMSD……Root Mean Square Distribution

Abstract

In this thesis computational modelling was used to investigate on the atomistic scale, the effects of external electric and electromagnetic fields (EMF) on protein behaviour and responses in an aqueous environment. The motivation behind this study is discussed in Chapter 1, along with a literature review on previous research on the effects of EMF on proteins, from both simulation based studies and experimental research.

Non-Equilibrium Molecular Dynamics was employed to simulate the protein response to external perturbations and the computational methodologies encompassing this technique are described in Chapter 2. The history of NEMD is also described in this chapter, along with the specific computational details for the simulation of our peptide model, apoC-II(60-70) exposed to EMFs of static/oscillating nature and different frequency and strength.

In Chapter we used all-atom NEMD simulations to understand and quantify the response mechanisms of the amyloidogenic apoC-II (60-70) peptides to non-ionising radiation by modelling their behaviour under static electromagnetic and electric fields of different strengths.

Chapter 4 expands on the previous study by investigating the role of the field frequency on the peptide behaviour in solution. Finally, Chapter 5 presents a summary of the conclusions drawn from this work.

Chapter 1
Introduction

1.1 Background

In this modern age, electromagnetic (EM) fields are becoming widespread, with existing and novel applications evolving constantly. While new (smart) mobile technologies continue to grow and reach the entire population of the planet, community concerns about their possible health effects are also growing. The consequences of exposure of basic biological systems, including water, proteins, DNA, cell membranes, and entire cells, to EM radiation in the radio frequency (RF) range have been a subject of intensive debate [1-8], but despite years of research, scientists and the public lack conclusive answers.

On the global level, concerns about EM field effects have been acknowledged by the World Health Organisation (WHO), a renowned group with a universal interest to ensure the safety of the public. The WHO also directs and coordinates research efforts world-wide on EM field exposure and guides policy standards. One such research group is the International Agency for Research on Cancer (IARC), which co-ordinated the largest case-control study to determine whether there are any links between mobile phone use and head/neck cancers in adults. The data from their study resulted in the new classification of EM field as a possibly carcinogenic (Group 2B) to humans, a category used when a causal association is considered credible, but chance, bias, or other variables cannot be ruled out with reasonable confidence [9].

In Australia, the National Health and Medical Research Council funded the Australian Centre of Excellence for Electromagnetic Bioeffects Research (ACEBR) (2013–2017) [10], which was recently renewed for another 5 years, which aims to address the WHO's research recommendations in order to better understand potential health effects of EM field exposure and protect the Australian community. The Centre involves research domains ranging from epidemiology, dosimetry, in vivo experiments (human and nonhuman), in vitro, and all-atom modeling projects, which this thesis forms part of.

The aim of this thesis is to investigate the molecular responses of an amyloidogenic peptide to EM radiation of different strength and frequency using Non-Equilibrium Molecular Dynamics (NEMD).

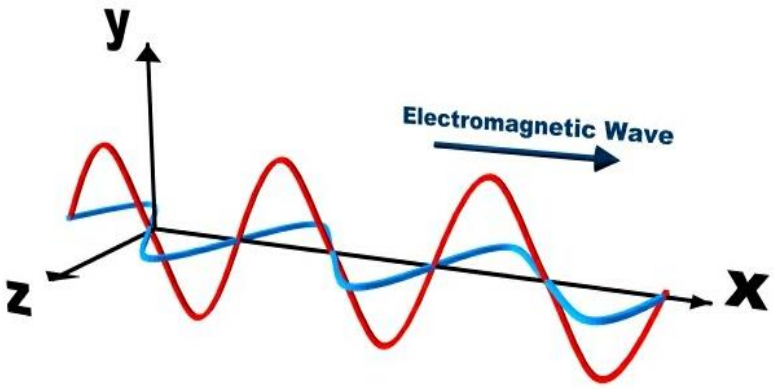

Figure 1: Electromagnetic wave diagram with electric field (red) and magnetic field (blue).

1.2 Electromagnetic Fields

EM fields are a mostly invisible form of energy, with a very small section of it being detectable by the naked eye, however years of research has revealed much about their form and function. They consist of two fields, an electric and magnetic field; radiating outwards from their source in orthogonal directions to each other and their source (see Figure 1).

These fields are characterised by their frequency and wavelength as ways of describing the fields in question.

- Frequency: The number of occurrences of a repeating event per unit of time. Specifically in EMF, it's the number of complete cycles the field makes in a second at each point in space. i.e. 1 Hertz (Hz) = 1 full cycle per second. 60 Hz = 60 cycles per second.
- Wavelength: The distance after which the oscillation repeats itself. Inversely proportional to the frequency; higher frequency = smaller wavelengths, and vice-versa.

The entire electromagnetic spectrum can be divided into several categories based on wavelength bands they occupy, however more broadly speaking, EM fields are generally referred to as ionizing, and non-ionizing fields.

Ionizing radiation (>950 THz) has the potential to induce cellular and DNA damage through the excitation of bonds, resulting in bond breaking, or the formation of free radicals within the body. The consequences of such effects have been known to result in cancers such as melanoma and glioblastoma, which is why human exposure to EM fields in this frequency range is limited [11].

Non-Ionizing radiation (<950 THz) is EM radiation hat does not carry enough energy per quantum (photon energy) to ionize atoms or molecules. The Radio Frequency range (20 KHz – 300 GHz) has been used increasingly for local and global communication, with mobile phones, Wi-Fi, and 'Smart' Meters being some of the main contributors to the increase in EM exposure. The emitted frequencies by some of these devices include:

(i) TV and PC monitors: 3 – 30 kHz;
(ii) Amplitude modulated radio emitters: 30 kHz – 3 MHz;
(iii) Induction heaters for industry: 0.3 – 3 MHz;
(iv) Mobile Phone Networks: 2G (900 MHz), 3G (850 – 2100 MHz), 4G (850 – 2600 MHz); 5G (1 – 100GHz)
(v) Microwave ovens: 2.45 GHz;
(vi) RADAR, Satellite Communications Systems: 3 – 30 GHz;
(vii) Solar radiations 30 – 300 GHz.

Due to the ubiquity of these fields, it is imperative to understand the mechanisms of interactions of such fields with biological matter.

1.3 EMF: a friend or foe to human health

The thermal effects of EM fields on macromolecules occurs through heat generation from the absorption of EM energy by the exposed matter. This process is well-known and utilised daily in kitchens everywhere through the use of microwave ovens, which heats food through the exposure of food and water to microwave energy that is absorbed and converted into vibrational energy, resulting in heating.

The non-thermal EM field effects are less well known [6, 12], however it has been suggested that EM fields are capable of exciting vibrational modes in proteins, causing structural

changes that can go on to alter their conformation and ultimately function [13-18]. These changes in conformation can lead to misfolding and aggregation of proteins into insoluble plaques.

The question of non-thermal effects on protein stability, and hence function, in far infrared and microwave fields has been the subject of extensive debate, particularly in relation to mobile communication signals on human health [19]. Owing in part to health problems of exposure to EM fields [5], there exists a body of experimental work on EM effects on protein denaturation and stability [20-22]. Other such reported incidents of negative EM field effects in humans include increases in cancer and glioblastoma occurrence [23], electro-hypersensitivity [24], and other deleterious effects [25-28], which will be discussed further in the next chapter.

EM fields have also been investigated for beneficial uses in medicine and industry. The medicinal uses of EM fields have been on non-invasive methods of treatment and prevention/treatment of various diseases, such as cancers [29] and Alzheimer's disease [30-32], and wound healing [33-35].

Extensive work has been performed by Arendash and co. [31, 36-38] on the effects of high frequency RF fields exposure on amyloid plaques found in the brains of Alzheimer's patients. Their research was performed on rats genetically predisposed to developing Alzheimer's like conditions, as well as common laboratory rats, and found that exposure to an appropriate field for 2 hours a day could not only prevent the development of Aβ plaques, but also be used to break up early formation of Aβ plaques. This apparently beneficial health effect, if substantiated, would suggest that our understanding EM field interactions with tissues is incomplete, and that potential novel applications of RF, including treatment of debilitating diseases, may emerge.

1.4 Protein structure

Proteins are important biological macromolecules that play many vital roles in living organisms, from enzymes and antibodies for digestion and immune response, to making up structural components of body tissues, such as muscle fibres. A protein is composed of amino acid residues that are joined via peptide bonds in a polymeric chain. There are 20 different

amino acids that occur naturally in proteins. Each amino acid is composed of a central carbon atom (Cα), attached to a hydrogen atom (H), an amino group (NH_2), and a carboxyl group (COOH). Individual amino acids are distinguished from one another by a unique side-chain (R) attached to the Cα through its fourth valence.

Amino acids are joined during protein synthesis by the formation of peptide bonds, linking the carboxyl group of one amino acid to the amino group of another. During this process a water molecule is lost. A polypeptide chain consists of a regularly repeating part, called the main-chain or backbone (NH–CαH–C'=O), and a variable R-group, comprised of distinctive side-chains. It is the chemical nature of the side-chain components of individual residues that determines the property of the protein. The properties are usually divided into three different groups.

- 1st: amino acids with strictly hydrophobic side-chains: Ala (A), Val (V), Leu (L), Ile (I), Phe (F), Pro (P), and Met (M);
- 2nd: the four charged residues: Asp (D), Glu (E), Lys (K), and Arg (R);
- 3rd: those with polar side-chains: Ser (S), Thr (T), Cys (C), Asn (N), Gln (Q), His (H), Tyr (Y), and Trp (W).

The amino acid Gly (G) is the simplest of the 20 amino acids; it has only a hydrogen atom as a side-chain, therefore has special properties and is usually considered to be a member of the hydrophobic amino acid group. Cysteine residues have a unique property in their ability to form disulfide bridges with another Cys side-chain in an oxidative environment. As the two cysteines are covalently bonded, the disulfide bond is very strong, and is essential for the folding, structure and function of a protein. In some proteins, these bridges hold together different polypeptide chains, such as the A and B chain of insulin, which are linked by two separate disulfide bonds.

Proteins are assembled from amino acids using the information encoded in our DNA (deoxyribonucleic acid). However, the process of protein synthesis is conducted over several important steps. Initially, the DNA transcribes a messenger RNA (mRNA) through *transcription*, where a small copy of a gene is released to the cytoplasm. Translation of the mRNA occurs in the ribosomes, located in the cytoplasm. During *translation*, the mRNA is decoded to produce a specific polypeptide chain according to rules specified by the genetic code. Shortly after or during synthesis, the residues in the proteins are often chemically

modified by *post-translational modification*, where the physical and chemical properties of the protein are altered, resulting in changes in the fold, stability and function of the protein.

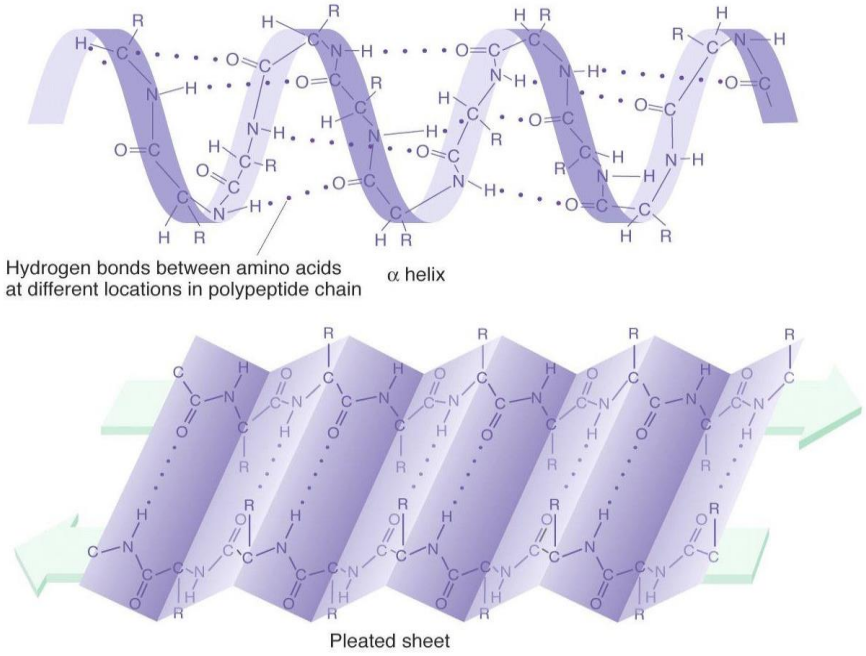

Figure 2: Protein secondary structure, (top) -helix, (bottom) beta pleated sheet [39].

The functional properties of proteins depend on their three-dimensional structure, which for convenience is represented in several structural levels. The amino acid sequence of a protein's polypeptide chain is called its *primary structure*. Different regions of the sequence form local regular *secondary structures*, such as α-helices or β-strands Figure 2. The three essential torsion angles: ϕ, ψ, and ω determine the conformation of the protein backbone. By convention, the angle of rotation around the N−Cα bond is called the phi (ϕ) angle, while the rotation around the Cα−C bond is called psi (ψ). The rotation around the C−N bond is called omega (ω), and this angle has a value close to 180° (except for *cis*-prolines, which have ω-angle close to 0°). The *secondary structure* is formed when consecutive residues have similar dihedral angle (ϕ, ψ) values that lie within known regions on the Ramachandran map [40], which is a plot used to visualise energetically allowed regions in protein structure. There are three sterically allowed regions on the Ramachandran plot. These regions correspond to secondary structures with well-defined dihedral angles: the right-handed α-helix, the left-

handed α-helix and the β-strand. The α-helix is a classical element of protein structure, and is easily recognised by its spiral-look. This structural motif is stabilised by the formation of parallel hydrogen bonds between the backbone atoms of consecutive residues in a protein. There are three types of commonly occurring helices: α-helix, 3_{10}-helix, and π-helices, all varying according to the hydrogen bond coordination of their backbone atoms, making the chain either more loosely or more tightly coiled.

The second major structural element found in globular proteins is a β-strand. The β-strand has a predisposition to self-associate and to form β-sheets, which are composed of several β-strands bound together by hydrogen bonds between the backbone atoms. The β-strands have an extended conformation, with average dihedral angles of (-120°, 120°), which belong in the broad region in the upper left quadrant of the Ramachandran plot. These strands interact in two ways to form pleated β-sheets: parallel and anti-parallel. The β-sheet structures are associated with the formation of amyloid fibrils, which are known to be the cause of many debilitating diseases.

Most protein structures are built up from a combination of secondary structure elements, such as helices and β-strands that are connected by turns and loop regions of various lengths and shapes. Loop regions that connect two adjacent anti-parallel β-strands are called β-hairpins. These structural elements are essential for protein folding and the formation of compact *tertiary structures*, as well as enabling flexibility in the protein, which is often related to its activity. The formation of tertiary structure is mostly driven by hydrophobic interactions between the secondary structure elements which minimise the solvent accessible surface area and increase the protein's conformational stability [41].

The arrangement of multiple folded protein molecules in a multi-subunit complex is referred to as a *quaternary structure*. An example is the insulin dimer that consists of two distinct monomer structures bound together by disulfide bonds, which combines further into a hexamer in the presence of metal ions, such as zinc.

The correct three-dimensional structure or native state is essential for protein function. Failure to fold into the native shape usually produces proteins with different properties that sometimes can be toxic, such as the prion-protein, which is associated with variant Creutzfeldt-Jakob disease. Several neurodegenerative and other diseases result from the accumulation of misfolded proteins.

1.5.1 Protein Folding and Aggregation

One of the most fundamental phenomena in nature is the capability of proteins to fold *de novo* to their native conformation, also known as their biologically functional state. While all the information needed for proteins to fold is encoded in their amino acid sequence, there are many more elements that play a part *in vivo*. In a crowded cellular environment, surrounded by interacting proteins, nascent polypeptides face a formidable challenge in finding the correct interactions that result in a folded and functional protein. Many become trapped in meta-stable intermediate structures, which are usually recognised by proteasomal machinery and degraded or refolded by chaperones. Alternatively, they can also misfold and self-associate leading to formation of either amorphous compounds or structures of elongated-unbranched morphology, known as amyloid fibrils. An accumulation of these fibrils can result in a range of human diseases commonly referred to as amyloidosis. Some of the diseases associated with amyloid fibrils are Alzheimer's, variant Creutzfeldt-Jakob disease, Parkinson's, type II diabetes and many others.

In 1935, Astbury and Dickinson placed a poached egg white in an X-ray beam and observed a diffraction pattern with perpendicular reflections at ~4.7 Å along the meridional direction and ~10 Å along the equatorial direction [42]. The pattern suggested that the protein chains of the egg white pack in an extended β-conformation, with the chains perpendicular to the long axis. This cross-β X-ray diffraction pattern was observed for the amyloid deposits in most diseased tissues. In 1959, Cohen and Calkins found that the amyloid, which is hyaline and structureless under light microscopy, in fact has a characteristic fibrillar ultrastructure when analysed with an electron microscope [43]. This finding was confirmed in several other studies [44-48], which gave further insight into the specific structural organisation of amyloid fibrils. Although the morphology of the fibrils is similar, consisting of a cross-β structure with the β-strands perpendicular to the fibril axis (Figure 3), the proteins from which they are built are different.

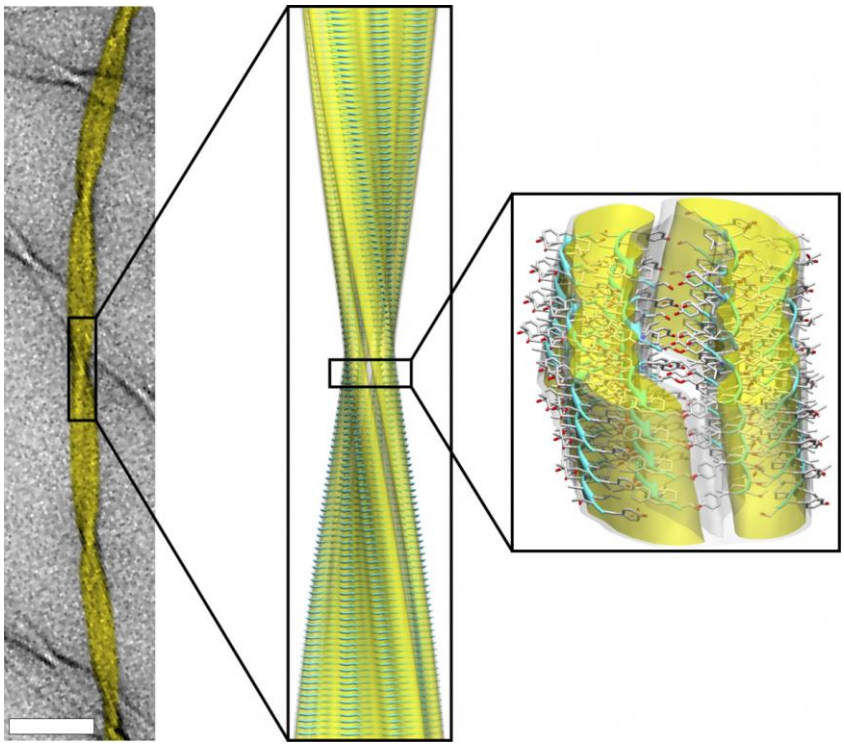

Figure 3: Background image of triplet TTR(105-115) fibril taken using TEM (*Left)*. TTR(105-115) triplet fibril fitted into cryo-EM reconstruction (*Center and Right).* [49]

Significant progress has been made in determining the structures of amyloid fibrils in atomic detail using experimental [50-53] and simulation methods [54-57] to improve the knowledge around how amyloid fibrils form and behave so that hopefully one day there will be treatments or preventative measures to their formation and the diseases that they cause.

1.6 Apolipoprotein C-II

The peptide model used in this thesis is apolipoprotein C-II (ApoC-II) derived peptide apoC-II(60-70), known to form fibrils in vivo [58-60]. ApoC-II is a 79 residue protein and a member of the very-low-density-lipoproteins (VLDL) [61]. It plays an important role in human physiology as an activator of lipoprotein lipase [62, 63]. Lipoprotein lipase is an enzyme found in the capillaries that catalyses the hydrolysis of triacylglycerols in chylomicrons to glycerol and fatty acids. Deficiencies in apoC-II have been associated with an elevation in triacylglycerol levels in the blood, which is consequently linked to atherosclerosis, and by extension, the risk of heart disease and stroke [64].

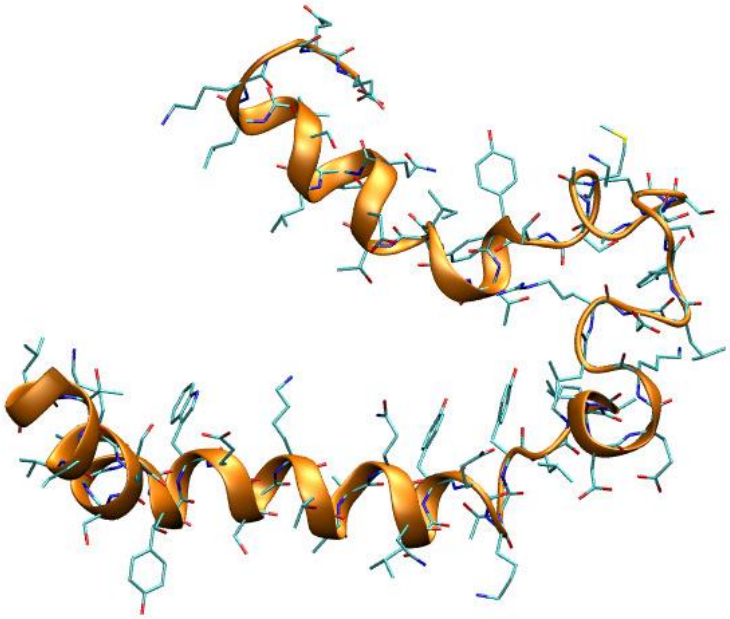

Figure 4: Ribbon representation of apoC-II(13-79) showing secondary structure and side-chains.

1.6.1 ApoC-II Structure

ApoC-II binds reversibly to the polar lipid surface of plasma lipoprotein particles *in vivo* and associates with a range of natural and synthetic lipid surfaces *in vitro* with an accompanying change in secondary structure. Analysis of this conformational change and the amino acid sequence of the lipid binding regions has led to the generally accepted hypothesis that apolipoproteins associate with lipid surfaces by means of amphipathic helices predicted to be present in all members of the family [65]. MacRaild and co-workers determined the lipid bound structure of apoC-II in the presence of dodecylphosphocholine micelles [66].

The primary sequence of human apoC-II is listed in Table 1. The region between residues 1 to 12 is highlighted in grey because the structure of this region was too difficult to assign [66, 67]. The secondary structure of apoC-II is well defined, with α-helical elements over most of the sequence, specifically between residues Leu15 to Lys39 and Tyr63 to Gly77. The central region, comprising residues Thr40 to Gly65 is substantially disordered, containing predominantly coil and turn structures. A representation of the secondary structure of apoC-II(13-79) is shown in Figure 4.

	1	**2**	**3**	**4**	**5**	**6**	**7**	**8**	**9**	**10**
0	Thr	Gln	Gln	Pro	Gln	Gln	Asp	Glu	Met	Pro
10	Ser	Pro	Thr	Phe	Leu	Thr	Gln	Val	Lys	Glu
20	Ser	Leu	Ser	Ser	Tyr	Trp	Glu	Ser	Ala	Lys
30	Thr	Ala	Ala	Gln	Asn	Leu	Tyr	Glu	Lys	Thr
40	Tyr	Leu	Pro	Ala	Val	Asp	Glu	Lys	Leu	Arg
50	Asp	Leu	Tyr	Ser	Lys	Ser	Thr	Ala	Ala	Met
60	Ser	Thr	Tyr	Thr	Gly	Ile	Phe	Thr	Asp	Gln
70	Val	Leu	Ser	Val	Leu	Lys	Gly	Glu	Glu	

Table 1: Primary sequence of apoC-II (PDB code 1SOH). The sequence coloured in grey represents the residues with undefined structure.

1.6.2 ApoC-II misfolding and aggregation studies

In the presence of lipids, apoC-II is comprised of mostly α-helical structures, however in lipid-poor conditions apoC-II readily aggregates into twisted ribbon-like fibrils. This protein is one of the few amyloid systems to form fibrils at physiological pH without prolonged agitation. ApoC-II and several other apolipoproteins have been identified in atherosclerotic plaques *in vivo* [64] and it is found colocalised in human coronary artery plaques with serum amyloid P, a non-fibrillar marker of amyloid deposits [62]. The fibrils formed by apoC-II *in vitro* are homogeneous when viewed by electron microscopy and display a characteristic X-ray diffraction pattern, indicating the formation of cross-β structure [68].

A unique property of mature apoC-II fibrils is that they are relatively small and remain soluble, allowing characterisation of fibril formation by analytical ultracentrifugation. Binger

and co-workers used this technique to show that mature fibrils assemble via a reversible pathway that includes fibril breaking and joining [69]. Solution conditions, such as the presence of auxiliary proteins [70], macro-molecular crowding agents [71] and the presence of phospholipids below and above the critical micelle concentrations alter the kinetics of apoC-II fibril formation and fibril morphology [51, 72]. Specifically, micellar phospholipid concentrations were found to inhibit apoC-II fibril formation, whereas sub-micellar concentrations accelerate the fibril forming process. Recent experimental work explored the effect of oxidation and mutation of methionine residues on the amyloidogenic nature of the protein [73]. Oxidation of the Met residues (Met9 and Met60) with hydrogen peroxide inhibited fibril formation. However, the oxidised monomers were found to have no effect on the already formed native apoC-II fibrils. This finding suggested that oxidised molecules have a reduced ability to interact with growing fibrils. Additionally, single Met60Val and Met60Gln mutations were also performed. The Met60Val mutant assembled into fibrils with similar kinetics to the wild-type apolipoprotein. In contrast, the Met60Gln mutant showed a significant delay in fibril formation when compared to the wild-type, however the fibril formation was not completely inhibited. This finding together with the oxidation of Met60 have showed that a change in hydrophobicity at a single position in the apoC-II core region is sufficient to significantly reduce the fibril-forming ability of this protein [73].

Wilson and co-workers performed hydrogen/deuterium exchange and proteolysis studies to identify the core region(s) within apoC-II fibrils that may stimulate amyloid formation [74]. The peptide fragments composed of residues 60 to 70 (Figure 5) and 56 to 76 have been shown to exhibit an inherent propensity for amyloid fibril formation in solution. The

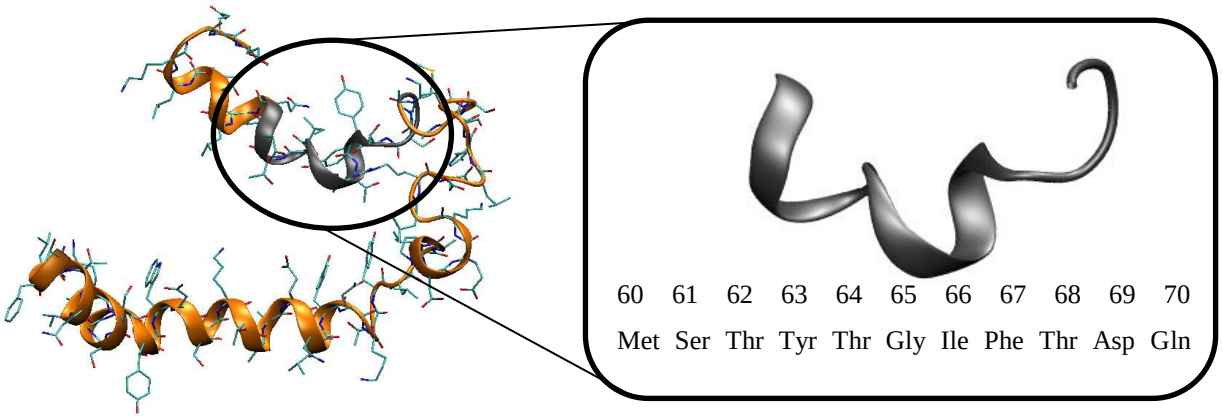

Figure 5: ApoC-II and the amyloidogenic peptide apoC-II(60-70) shown as inset (black).

synthetic apoC-II(56-76) readily formed fibrils, although with a different morphology and thioflavin T fluorescence yield compared to full-length apoC-II. Furthermore, Wilson *et al.* postulated that the ability of apoC-II(60-70) to independently form amyloid fibrils may be the underlying cause of apolipoproteins and their peptide derivatives to accumulate in amyloid deposits *in vivo* [74].

The amyloidogenic properties of apoC-II have been extensively studied *in vitro* and these studies form the basis for much of the current knowledge of amyloid fibril formation by apolipoproteins [75]. Recently, *in silico* studies were performed to gain insight into the atomistic detail of the dynamics and association in various environments of apoC-II peptides.

The small size and amyloidogenic nature of the apoC-II(60-70) peptide were the driving motivation behind the extensive theoretical and experimental studies of this peptide in ambient and various experimental conditions in our group [57-60, 76-78, 81, 82, 84]. Our simulations identified the fibrillation propensities of apoC-II(60-70) under varying pH, different degree of oxidation, mutations, lipid concentrations, and in the proximity of nanoparticles [79, 85]. As an example, at fibril-favouring conditions (neutral and low pH) the peptide preferentially adopts structures similar in shape to a β-hairpin, while under fibril-disruptive conditions (lipid-rich and oxidised Met) significantly different structures were obtained. The formation of a strong hydrophobic core, as exhibited in a β-hairpin structure (Figure 6), have been suggested favourable for peptide interaction and subsequent fibril formation [74, 78]. Using these extensive benchmarking data on this peptide, we present a systematic study of the EMF effects on the structure, dynamics of the amyloidogenic apoC-II(60-70).

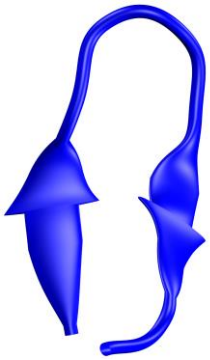

Figure 6: The apoC-II(60-70) peptide has been shown to adopt a β-hairpin conformation under fibril favouring conditions [52, 54, 57, 60, 76-83].

1.8 Literature Review on Computational Modelling Studies of Biomolecule Responses to Electric Fields

Tekieh et al [86] studied the effects of an EM field on voltage gated ion channels, as dysfunction in calcium ion channels can lead to diseases such as absence seizures, cerebellar ataxia, familial hemiplegic migraine, and many more. They found, that the ionic current of the ion channel changes under an EM field, suggesting that EM radiation can help ions to climb over barriers and enter ion channels more quickly, which as they stated could result in deleterious effects of seizures and migraines, however this could also indicate a possible medical application for ensuring the uptake of drugs into specific areas or tissues of the body, such as cancerous cells and tumours, and this lack of deeper investigation can end up fuelling even more fear of EM fields.

Toschi et al. studied the interactions of β-amyloid (Aβ(1-40)) and applied electric field of varying strengths (0.1 – 1.0 V/nm) [87]. The simulation of applied electric field to the protein saw that the presence of external electric field was able to facilitate the process of α-helix conversion to random coil and/or β-secondary structures. When the field was turned off, they observed that the α-helix to β-sheet conversion would not revert and instead observed the formation of β-bridges, however due to the relatively short time scales of MD simulations they were not able to observe if there was any instances of β-sheets converting back into α-helixes. Toschi et al. also only performed simulations where the electric field was present then turned off, meaning that we cannot know if the presence of a permanent electric field, or having the field switched on again would cause different results or affect the protein structure further.

Marrachino et al. investigated the structural response of myoglobin to a static electric field and to a pulsed electric field of 8 ns at 0.1 and 1.0 V/nm [88]. They found that 1.0 V/nm fields caused the myoglobin to undergo a fast unfolding transition, characterised by an intense polarisation, which was the cause of the denaturation. The 0.1 V/nm field, on the other hand, still experienced a significant polarisation and affected the myoglobin dipole moment, but no denaturation was observed, indicating that minimum field strengths are needed to cause protein denaturation. Their simulations of pulsed electric fields also saw changes from their null field simulations however there is a lack of interpretation of these results within the article to be able to make any comments on them.

Comprehensive research by English et al. has been performed to simulate the effects of electric fields and EM fields on water [89-91], exploring how EM field affects the cohesion of water molecules [89, 90]. They were able to effectively simulate the effects of EM field on water molecules and show that a polarizable water model was more appropriate to use for accurate replication of EM field effects than a non-polarizable one.

The team also explored the effects of EM fields on proteins, Specifically, the hen egg white lysozyme (HEWL) [14, 15, 92] was simulated under EMF of 50 to 500 GHz and 1.0 to 5.0 V/nm_{rms}, then compared to thermal effects on HEWL. Their study showed that 5.0 V/nm_{rms} EM field caused denaturation to the protein greater than being exposed to 500 K. English et al. then went on to simulate HEWL under 2.45 GHz fields at various strengths (0.1 to 1.5 V/nm_{rms}). Under these field conditions they again saw significant changes in the protein's secondary structure, with charged residues undergoing more localised motion. English et al. also noted that these secondary structure changes seemed to occur primarily due to the peptide dipole alignment with the applied external field.

Human aquaporin (h-AQP) [93-95] are transmembrane proteins that form channels which conduct water and small uncharged molecules through them. English et al. simulated these protein channels under EM field to see how the presence of external fields (0.065 V/nm_{rms} and 2.45 to 100 GHz) in the –z (pore axis) and –y (orthogonal to the pore axis) directions changed the flow of the channel [93] and found that applied EM field could disrupt the water dipole orientation, which in turn lowered the permeability of the membrane. A follow up simulation [94] of EM field and h-AQP was performed with 0.065 V/nm_{rms} and 2.45 and 100 GHz fields along the same directions as the previous work, and found that the dipole orientation of Histidine-201 residue in the selectivity filter which governs the dihedral angle, and thus influences water self-diffusion. A more recent study [95] on h-AQP under EM field was performed, using the same field strength as the last two studies, and a frequency range of 2.45 to 500 GHz, but this time in the –z and +z directions, while the previous two studies only used the –z direction, and found that the application of EM field in the +z direction would cause the channel to open two areas of the pore that have been proposed as a two-stage filter, which may result in the pore malfunctioning and causing unseen health problems.

English and Waldron also published a comprehensive review article on EM field effects on macromolecular systems covering a plethora of published articles that focussed on electric and EM field effects and the challenges that are still facing researchers to this day [7].

Previously in our group, Budi et al. performed molecular dynamics studies on insulin chain-B, and full insulin peptide, to investigate the effect of electric fields on protein conformation [2, 3, 96]. These studies used a range of strengths (0.01–1.0 V/nm) and frequencies (static, 1.225, 2.45, 4.9 GHz). Their studies found that the application of a static electric field (1.0 V/nm) to the insulin chain-B peptide was able to cause structural disruption, while the use of an oscillating field resulted in destabilisation at a lower field strength (0.5 V/nm). When they simulated the full insulin protein [3], Budi et al. found that the presence of chain-A strengthened the protein against thermal stresses, but the addition of extra protein dipoles meant that the protein was more susceptible to the external fields, which caused denaturation at a lower field strength, but with an increase in lag time, as the dipoles all attempted to align with the field independently.

1.9.0 Research Goals

The aim of this project is to use molecular dynamics techniques to investigate the effects of electric and EMF on the apoC-II(60-70) peptide derivative. The peptide behaviour exposed to fields of different strength and frequency are investigated. The specific research questions for the project are listed below:

1. What are the magnetic field contributions in simulations of external electromagnetic field compared to electric field only simulations?

2. Considering the current state of the art in the all atom simulations is to model proteins in solution for up to several microseconds, what is the lowest field strength which will affect the structural integrity of apoC-II (60-70) peptide within a microsecond time frame?

3. How do different frequencies of EM fields (in the RF range) affect apoC-II(60-70) peptide structure and dynamics?

4. Is there in fact a correlation between e/m field strength/frequency and protein response?

Chapter 2
Theory of EMF Molecular Modelling

2.1 Molecular Mechanics

Molecular modelling is a collective term for theoretical methods and computational techniques that are applied to mimic or model the behaviour of molecules, ranging from small chemical systems to large biological molecules or material assemblies. While experiments are useful in determining many properties of different materials, they are still very limited in studying phenomena at atomic resolution within short time-scales at various environmental conditions. An advantage of computer simulations over traditional experimental methods is the ability to characterise the time evolution of a system under controlled conditions at atomistic detail.

Today computer simulation techniques can be classified into several categories based on the studied system size and time-scale capabilities. The most accurate methods are based on Quantum Mechanics (QM), and comprise the *ab-initio* and Density Functional Theory (DFT) methods. Protein models are too large to be treated by these techniques as the properties of the system are calculated from first principles, i.e. considering the electronic structure, which is computationally prohibitive for proteins. A less expensive approach is offered by the *semi-empirical methods* which allow for larger systems to be simulated at the electronic level, treating only the valence electrons explicitly and fitting several parameters to experimental data. However, the QM methods are mostly used for investigating processes which involve bond breaking and forming, electronic rearrangement, and force field parameterisation.

Larger system sizes and longer simulation time scales can be investigated using the atomistic force field methods or molecular mechanics. The main concept behind this method is the *Born-Oppenheimer approximation*, which allows for the expression of the electronic movement to be separated from the Hamiltonian of the system, allowing the electronic and

the nuclear variables to be calculated separately. Molecular mechanics is used when physical interactions are considered (as opposed to chemical) and based upon a simpler model of interactions within a system with contributions such as stretching of bonds, the opening and closing of angles (angle bending) and rotations about single bond (torsions). This method can provide accurate calculation of physical phenomena such as protein dynamics, in a fraction of the computer time compared to *ab-initio* calculations.

Furthermore, coarse-grained mechanics has the ability to simulate large complexes at timescales currently inaccessible to atomistic methods. These methods can also provide qualitatively accurate representation of the macroscopic states and some properties of a system over long time scales. In a coarse-grained model a small group of atoms is treated as a single interactive unit, or bead, where the dynamics of the system is governed by a very simple force field. There is an intrinsic difficulty in the parameterisation of coarse-grained force fields, related to the fact that complex and diverse interactions must be described by a small number of parameters. However, continued development and improvements of different coarse-grained models means this method has great potential for modelling large complex systems comparable with those found in experiments.

2.2 Potential Energy Functions

Fundamental to molecular mechanics simulation methods are the forces that govern the atomic motions and pair-wise atom-atom interactions. These forces are described by empirical or QM derived potential energy functions. The combination of the potential energy function with the geometric and energetic parameters used, yield what is known as a force field (FF). FF's are usually developed in the context of a specific environment, such as biological milieu which includes water, ions, and macromolecules (proteins, lipids, and DNA). Many of these FF's have been specifically developed to replicate experimental data associated with the behaviour of water in these biological environments. Several different types of water models exist, fitting into 3 groups, the simple rigid water models, flexible water models, and models that explicitly include the effects of polarisation. The simple rigid water models typically use between three and five interaction sites, TIP3P and SPC are commonly used 3 site models. FFs that have been developed to enable an accurate description of proteins in these explicitly solvated environments include the all-atom

CHARMM, AMBER FFs that were developed with the TIP3P water model and the all-atom OPLS-AA and united-atom GROMOS FFs, which were parameterised with the SPC water model. The all-atom FFs, as the name suggests, describe every atom explicitly, while the united-atom FFs treat hydrogens bonded to an aliphatic carbon as a single interaction site, which can reduce the computational cost of these simulations.

The functional form of each force field contains energy terms describing the bonded (E_{bonded}) and nonbonded ($E_{nonbonded}$) interactions between the atoms of a system. The terms representing bonded interactions account for the stretching of bonds, the bending of valence angles, and the change in the dihedrals produced by the rotation.

$$E_{bonded} = \sum_{bonds} K_b(b - b_0)^2 + \sum_{angles} K_\theta(\theta - \theta_0)^2 + \sum_{dihedrals} K_\chi(1 + \cos(n\chi - \sigma))$$

The nonbonded terms represent the electrostatic and van der Waals interactions.

$$E_{nonbonded} = \sum_{non\ bonded\ pairs\ ij} \left(4\varepsilon_{ij} \left[\left(\frac{\sigma_{ij}}{r_{ij}} \right)^{12} - \left(\frac{\sigma_{ij}}{r_{ij}} \right)^{6} \right] + \frac{q_i q_j}{4\pi\varepsilon_0 r_{ij}} \right)$$

The total potential energy function is in the form of:

$$E_{total} = E_{bonded} + E_{nonbonded}$$

where E_{bonded} is the contribution from the bonded interactions, $E_{nonbonded}$ is the contribution from the nonbonded interactions, to the total energy.

The first term in the equation describes the stretching of bonds summed over all bonded pairs, where each bonded pair is represented by a Hooke's law formula. K_b and b_0 are the parameters describing the stiffness and reference bond length respectively, and b represents the interaction distance between atom pairs. The second term is also represented by a triplet of bonded atoms. Similar to the bonded term, K_θ and θ_0 are the parameters describing the stiffness and reference angle position, respectively, while θ represents the angle formed by the three consecutively bonded atoms. The final term describes the change in the dihedral produced by the rotation around the central bond of any four consecutively bonded atoms; these rotations are a periodic function described by the cosine function. K_χ, n, and σ represent the barrier height for the rotation around the central bond, the periodicity, and the phase respectively.

The nonbonded potential energy equation, describes the intermolecular or nonbonded interactions. Generally, nonbonded interactions between atoms are calculated between atoms in separate molecules or between atoms separated by three or more bonds in the same molecule. The first part of the equation is the van der Waals term, described by the Lennard-Jones equation, which models the attractive dispersion and repulsive interactions. The ε_{ij} parameter is the well depth of the interaction between atoms i and j, r_{ij} is the distance between the two interacting atoms, σ parameter defines the separation for which the Lennard-Jones energy is zero for the combination of atoms i and j, which is also known as the collision diameter. The second part of the nonbonded energy equation models the electrostatic interactions between the nonbonded pairs of atoms. The electrostatic interactions are based on Coulomb's law, where the product of the particle charges of the atoms i and j, that is q_i and q_j, divided by the separation distance of the two atoms and the dielectric properties of the medium ε_0 results in the electrostatic contribution to the nonbonded energy. The partial charges on these atoms are noninteger values that are selected to represent the overall charge distribution of a molecule. The sum of the partial charges in a molecule must equal the molecules' net formal charge. While the previous applies generally to all FF's there are some variations that are important to consider. One important difference between FF's is the variable of "improper" dihedrals, which can be applied to maintain chirality or planarity at an atom centre bonded to three other atoms, an example is for cyclic molecules like benzene. The CHARMM and GROMOS FF's add a separate term for improper dihedral energy that has a quadratic dependence on the value of the improper dihedral, similar to the terms for bonds and angles. The additional separate term is important for the united-atom GROMOS FF, as it does not include particle positions for the hydrogen atoms bonded to aliphatic carbons, the improper dihedral term serves to preserve chirality at these carbon centres.

The energy functions discussed above are not of any value if they are not accompanied with a set of parameters that describe the energetic and geometric properties of the interacting particles. The optimisation of force field parameters involves adjusting the parameter values so the force field is able to reproduce experimental data. This may include the use of experimental spectroscopic, thermodynamic, and crystallographic data as well as data computed using quantum mechanics methods. Typical examples of experimental data used for parameterisation of a force field or the consequent refinement are: vibrational spectra, densities, solvation free energies, electron, or X-ray diffraction structures, and relative

conformational energies and barrier heights. The most commonly used force fields are the AMBER, CHARMM, OPLS-AA, and GROMOS force fields, each based on a different type of experimental data, although there is some overlap. The parameters for these force fields were extensively optimised with particular emphasis on the treatment of proteins.

An essential aspect of the use of a force field for biomolecular simulations is the accurate treatment of the condensed aqueous environment. When selecting a water model to use for a particular study, the most important consideration is its compatibility with the biomolecular force-field used. The reason for this is that most force fields have been developed in conjunction with a specific water model. For example, AMBER, CHARMM and OPLS have been developed with the TIP3P water model, OPLS also with TIP4P while GROMOS with SPC and F3C models. The most commonly used water models are TIP3P and SPC models.

For the studies in this thesis, the GROMOS force field parameter set 43A1 and SPC water model were used which emulated the structural features of the protein of interest as seen in experiments [52, 78, 80].

2.3 Molecular Dynamics

The molecular dynamics simulation technique is one of the most important and widely used method for studying the structural time evolution of many particle systems at atomic detail. The first molecular dynamics application was performed by Alder and Wainright [97, 98] on a system of hard spheres, as a model for atomic-scale systems. This was the first application of molecular dynamics and since then it has been applied in a variety of systems, including polymers, nano-materials and different biological composites of various size. A comprehensive review on some of the application of molecular dynamics can be found in reference [99].

2.3.1 Equations of Motion

The molecular dynamics simulation method is based on Newton's law of motion, $F = ma$. By solving the differential equations embodied in Newton's second law, we are able to obtain a

trajectory that describes the positions, velocities and accelerations of the particles as they progress over time.

$$\mathrm{F}_i = \frac{dE}{d\mathrm{r}}$$

$$\frac{\mathrm{F}_i}{m_i} = \frac{d^2 r_i}{dt^2}$$

The force $\mathbf{F}_i$ acting on the particles in the system is derived from the potential energy $E(r^N)$ which is defined by the selected force field, where $r^N = (r_1, r_2, r_3 \ldots r_N)$ represents the complete set of 3N atomic coordinates. Even though the equation is simplistic in its form, there is no analytical solution to the equation of motion for systems of more than two particles, so it must be solved numerically. Numerous algorithms have been developed for solving these equations, and most are derived from the widely used Verlet algorithm [100], with variations including the leap-frog algorithm [101], velocity Verlet [102] and Beeman's algorithm [103]. All algorithms assume that the positions and dynamic properties can be approximated as Taylor series expansions.

2.3.2 Periodic Boundary Conditions

One of the limitations of computational methods is the inability to effectively simulate large systems over long periods of time, although sometimes this is necessary depending on the problem to be investigated. The correct treatment of boundaries and border effects is crucial to simulation methods because it enables "macroscopic" properties to be calculated from simulations using a relatively small number of particles. The traditional way to minimise the edge effects in a finite system is to apply periodic boundary conditions in such a way that the particles experience forces as if they were in bulk fluid. The atoms of the system to be simulated are placed into a space-filling box, which is surrounded by translated copies of itself. In the two-dimensional example each box is surrounded by 8 neighbours; while in three dimensions each box would have 26 nearest neighbours. The coordinates of the articles in the image boxes can be computed by adding or subtracting integral multiples of the box sides. If a particle leaves the box during the simulations, it will be replaced by an image particle that enters from the opposite side. The number of particles within the central box thus remains constant.

Depending on the system to be examined, there are several space-filling type boxes that may be more computationally efficient for running molecular dynamics calculations. There is the cubic unit cell, rhombic dodecahedron, truncated octahedrons, and the most general space-filling shape, the triclinic unit-cell [104]. A typical triclinic simulation box containing a model protein in explicit solvent is presented in Figure 7.

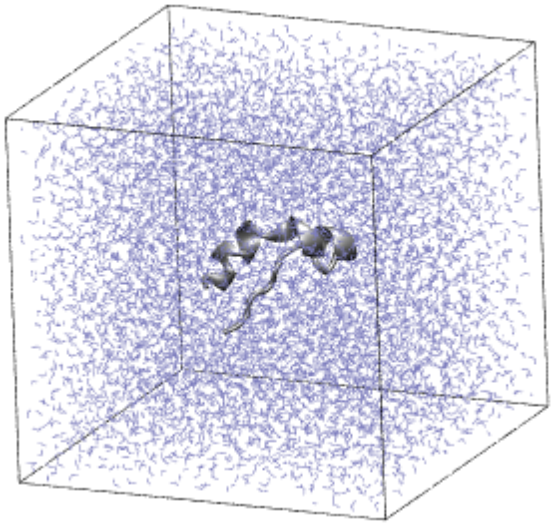

Figure 7: Three-dimensional representation of a typical simulation box with solvent and protein model shown explicitly.

2.3.3 Neighbour search and nonbonded interactions

The most time consuming part of a molecular dynamics simulation is the calculation of the nonbonded energies and forces, also known as the long-range electrostatic and Lennard-Jones effects. The most popular approach to deal with the nonbonded interactions is to apply the minimum image convention [105] where the nearest image of each particle is considered for calculation of the short-range nonbonded interaction terms. Another approach is to implement the nonbonded cutoff or potential truncation method. When a cutoff is employed, the interactions between all pairs of atoms that are further apart than the cutoff value are set to zero. This is because the greatest contribution to the potential and forces comes from the neighbouring particles, therefore only the closest image is taken into account. The potential truncation method introduces a small perturbation to the potential and force calculations, rendering it not accurate enough for calculations of long-range electrostatic interactions, and

can become computationally expensive as the system size increases. To lessen the computational burden, various truncation schemes have been developed whereby nonbonded interactions beyond a cutoff distance are ignored, and a smoothing function is typically applied to ensure continuity in the forces [106]. Such procedures imply severe approximations in the case of electrostatic interactions with energy decaying as $1/r_{ij}$. As a result, these interactions continue to make a substantial contribution to the total system energy beyond the typical cutoff length of approximately 10 Å. When periodic boundary conditions are being used the cutoff should not be so large that a particle sees its own image or the same molecule twice. This has the effect of limiting the cutoff to no more than half the length of the cell when simulating atomic fluids.

The introduction of Ewald sums [107] into biomolecular simulations under periodic boundary conditions has solved some of the problems associated with cutoff methods. The system is treated as being infinitely periodic, and interaction energies and forces beyond the cutoff length are calculated using the Ewald algorithm. This method works in reciprocal space, instead of being calculated directly using Coulomb's law. Although the original Ewald formalism is computationally expensive, recent developments based on grid-based treatments of reciprocal space, including Particle-Mesh Ewald (PME) methods [108], allow for the rigorous treatment of long-range electrostatics in a computationally efficient manner [109, 110].

2.3.4 Thermodynamic Ensembles

The simplest MD simulation of a system under periodic boundary conditions is evolved under constant energy and constant volume conditions (NVE). Although thermodynamic results can be transformed between ensembles, this is strictly only possible in the limit of infinite system size, also known as "the thermodynamic limit". It may therefore be desired to perform the simulation in a different ensemble, such as the canonical ensemble (NVT) and isothermal-isobaric ensemble (NPT). Additionally, many experimental measurements are made in environments of constant temperature and pressure, and so simulations in the isothermal-isobaric (NPT) ensemble are more directly relevant to experimental data.

2.3.5 Temperature Coupling

For several reasons such as solute drift during equilibration, drift as a result of force truncation, and integration errors, heating due to external or frictional forces, it is necessary to control the temperature of a system. The weak coupling scheme of Berendsen [111] and the extended-ensemble Nosé-Hoover scheme [112, 113] are the two most widely used temperature coupling methods.

The Berendsen temperature coupling algorithm mimics weak coupling with first-order kinetics to an external heat bath with a given temperature T_0. The effect of this algorithm is that a deviation of the system temperature from T_0 is slowly corrected according to

$$\frac{dT}{dt} = \frac{T_0 - T}{\tau}$$

which means that a temperature deviation decays exponentially with a time constant τ. This method of coupling has the advantage that the strength of the coupling can be varied and adapted depending on the simulation requirements. For example, for equilibration purposes the coupling time can be set quite short (e.g. 0.01 ps), with minimum influence on the system's dynamics. The heat flow into or out of the system is effected by scaling the velocities of each particle every step with a time-dependent factor λ, given by

$$\lambda = \left[1 + \frac{\Delta t}{\tau_T}\left\{\frac{T_0}{T\left(t - \frac{\Delta t}{2}\right)} - 1\right\}\right]^{1/2}$$

The τ_T is close to, but not exactly equal to the time constant τ of the temperature coupling. This is because the kinetic energy change caused by scaling the velocities is partially redistributed between the kinetic and potential energy, and hence the change in temperature is less than the scaling energy. In practice, the scaling factor λ will always be closer to 1. The Berendsen weak coupling algorithm is extremely efficient for relaxing a system at a target temperature.

A method which gives correct description for canonical ensemble simulations is the extended-ensemble approach first proposed by Nosé [112] and later modified by Hoover , now known as the Nosé-Hoover temperature coupling algorithm. In this method, the system Hamiltonian is extended by introducing a thermal reservoir and a friction term in the

equations of motion. The friction force is proportional to the product of each particle's velocity and friction parameter ξ. This friction parameter, or 'heat-bath' variable, is an independent dynamics quantity with its own equation of motion, where the time derivative is calculated from the difference between the current kinetic energy and the reference temperature. In Hoover's formulation, the particles' equations of motion from the equation are replaced by

$$\frac{d^2 r_i}{dt^i} = \frac{F_i}{m_i} - \xi \frac{dr_i}{dt}$$

Where the equation of motion for the motion for the heat bath parameter ξ is given by

$$\frac{d\xi}{dt} = \frac{1}{Q}(T - T_0)$$

In the equation above, T_0 denotes the reference temperature, while T is the current instantaneous temperature of the system, and Q determines the strength of the coupling.

Overall it is important to keep in mind the difference between the weak coupling scheme of Berendsen and the Nosé-Hoover algorithm. When applying the weak coupling scheme a strongly damped exponential relaxation is obtained, while the Nosé-Hoover approach produces an oscillatory relaxation. This means that the actual time it will take to relax the system with Nosé-Hoover coupling could be several times longer than the period of oscillations selected, which is important to note in the set-up stage of molecular dynamics simulations.

2.3.6 Pressure Coupling

With similar reasoning to that behind the need for temperature coupling, a system can also be coupled to a pressure bath to give the correct representation of a molecular system. The two most widely used methods are the Berendsen algorithm [111] and the extended-ensemble Parrinello-Rahman approach [114]. A key advantage of these methods is that they can be combined with any of the temperature coupling methods described previously.

The *Berendsen pressure coupling* algorithm rescales the coordinates and box vector every step with a matrix **μ**, which has the effect of a first-order kinetic relaxation of the pressure towards a given reference pressure $\mathbf{P}_0$:

$$\frac{d\mathbf{P}}{dt} = \frac{\mathbf{P}_0 - \mathbf{P}}{\tau_P}$$

The scaling matrix **μ** is given by

$$\boldsymbol{\mu}_{ij} = \delta_{ij} - \frac{\Delta t}{3\tau_P}\beta_{ij}\left[\mathbf{P}_{0ij} - \mathbf{P}_{ij}(t)\right]$$

The β value in the equation represents the isothermal compressibility of the system, where for water at 1 atm and 300 K, $\beta = 4.6 \times 10^{-5}$ bar^{-1}. Most other liquids have similar compressibility values. In the Berendsen algorithm the velocities of the system are neither scaled nor rotated.

For correct calculation of thermodynamic properties the fluctuations in pressure or volume are important, so it is advisable these are correctly represented in the ensemble simulated. This can be achieved using the *Parrinello-Rahman* approach, which is similar in form to the Nosé-Hoover temperature coupling method. With the Parrinello-Rahman barostat, the box vectors are represented by the matrix **b**.

$$\frac{d\mathbf{b}^2}{dt^2} = V\mathbf{W}^{-1}\mathbf{b}'^{-1}(\mathbf{P} - \mathbf{P}_{ref})$$

The volume of the box is denoted V, and W is a matrix parameter that determines the strength of the coupling. The matrices **P** and $\mathbf{P}_{ref}$ are the current and reference pressures, respectively. The equations of motion are also changed, just as for the Nosé-Hoover temperature coupling.

$$\frac{d^2\mathbf{r}_i}{dt^i} = \frac{\mathbf{F}_i}{m_i} - \mathbf{M}\frac{d\mathbf{r}_i}{dt}$$

$$\mathbf{M} = \mathbf{b}^{-1}\left[\mathbf{b}\frac{d\mathbf{b}'}{dt} + \frac{d\mathbf{b}}{dt}\mathbf{b}'\right]\mathbf{b}'^{-1}$$

Overall, by implementing the Parrinello-Rahman barostat in combination with the Nosé-Hoover thermostat an accurate isothermal-isobaric ensemble can be generated. Similar to the Nosé-Hoover thermostat, Parrinello-Rahman coupling gives oscillations of the unit-cell vectors. Berendsen coupling on the other hand, has the advantage that the fast kinetics of the

system will be unaffected and the disadvantage that it is unknown if the desired ensemble will be generated.

2.3.7 Bond Constraint Algorithms

As previously discussed, one of the most demanding aspects of a simulation is the computation of nonbonded interactions because for some large systems, millions of pairs have to be evaluated for each time step. One way to enhance computational efficiency is by extending the time step used for each calculation. However, this will introduce systematic errors, as the shortest timescale in biological simulations are the hydrogen bond vibrations at 1 fs. Fortunately, in most simulations the bond vibrations are not of interest per se, and can be removed entirely by introducing bond constraint algorithms such as SHAKE [115] or LINCS [116]. Constraints make it possible to extend time steps to 2 fs.

The most widely used algorithm for large molecules is SHAKE, in which the bonds and angles are reset to prescribed values by moving the bonded particles parallel to the old bond directions. SHAKE is an iterative method, where all the bonds are reset sequentially to the correct length. Because the bonds are coupled, this procedure has to be repeated until the desired accuracy is reached. SHAKE is simple, and numerically stable since it resets all constraints within a prescribed tolerance; however this method has the drawback that solutions may not be found when displacements are large. This is due to the coupled bonds being handled one by one, thus correcting one bond may tilt a coupled bond so far that the method does not converge.

A fast, reliable Linear Constraint Solver (LINCS) algorithm for molecular simulations was developed by Hess et al. where the constraints themselves are explicitly reset instead of the derivatives of the constraints [116]. The derivation of the algorithm is presented in terms of matrices; however no matrix multiplications are needed, making the method applicable to very large molecules. Although the LINCS algorithm shows the same accuracy as SHAKE, it is three to four times faster [116].

2.4 Non-Equillibrium Molecular Dynamics

The application of external perturbations to classically-propagated systems interacting with force fields represents, also referred to as Non-Equillibrium Molecular Dynamics (NEMD), has had a broad and rich history in MD. If explicit point charges at sites are missing, it will not be possible for the field to couple with the system, unless explicit dipoles are put in place on some or all particles, using the dipole formulation of electrostatics [117]. Although a more general discussion of NEMD is beyond the scope of this thesis, the general concept is to apply a forcing function to the system Hamiltonian

$$H_{\mathrm{E}}(t) = -\boldsymbol{\mu}_{\mathrm{tot}} \cdot \mathbf{E}(t) = -\mu_{tot,z} E(t) \qquad (1)$$

or, equivalently, the equations of motion,

$$m_i \ddot{\mathbf{r}}_i = \mathbf{f}_i + q_i \mathbf{E}(t) + q_i v_i \times \mathbf{B}(t) \text{ where } \mathbf{f}_i = -\nabla_{r_i} V \qquad (2)$$

$$\mathbf{E}(t) = \mathbf{E}_{max} cos(\omega t)\mathbf{k} \text{ and } \mathbf{B}(t) = \mathbf{B}_{max} cos(\omega t)\mathbf{j} \qquad (3)$$

Earlier attempts in NEMD were motivated by the desire to estimate transport coefficients, given that the use of linear-response theory or time-correlation functions can be subject to statistical error; these have included shear flow, heat and mass flow, as discussed in more detail by Evans and Morriss [118, 119] and Hanley [120]. The intellectual foundation of the type of external electric-field forces applied to point charges (cf. eqn (2) and (3)) dates back 40 years to 1975 in Ciccotti and Jacucci's seminal study [121], wherein an external force was applied to charged Lennard-Jones particles under periodic boundary conditions (PBC) to induce translational motion and record steady-state drift velocities. In a subsequent visionary article, Ciccotti et al. then performed NEMD using a Hamiltonian perturbation similar to eqn (1) (with resultant E forces as in eqn (1) and (3)), except with the result of induced translational motion of oppositely-charged ions in a binary electrolyte solution in opposing directions [122]; this field form also allowed for time-dependence [122], 'paving the way' for future work in alternating electric and EM fields. Heyes and Clarke also applied static fields to KCl electrolytes in contact with rigid surfaces via MD in 1981 [123], noting charge separation. These early studies were the first de facto ones with external electric fields applied, albeit to induce translational motion in explicitly-charged particles (with no dipoles).

2.4.1 Electromagnetic Field Modelling Studies

In 1982‑1983, Evans [124-128], and Evans and Powles [129], were the first to report the application of electric fields to model dipolar liquids under PBC (with each overall particle or molecule being electroneutral but explicitly dipolar), rather than as explicitly charged overall [121, 122]; Evans and Powles considered the example of a diatomic, hydrogen chloride, with individual atomic point charges [129] heralding the first example of combined explicit rotational and translational motion in an external electric field. These studies [124-129] were for pure electric fields, primarily static in nature, although also discussing alternating (similar to E in eqn (3)) [126, 127] and this field coupling (along the lines of eqn (1)‑(3)) induces rotational motion directly via an applied (formal or de facto) torque [124-129], albeit roto-translational coupling will serve inevitably to induce some degree of 'secondary' translational diffusive motion. The transient and steady-state dipolar response, inter alia, was studied [124-129]. Building on the foundations of time-varying fields of Ciccotti et al. in the late-1970s [122] and Evans in the early- to mid- 1980s [126, 127] Zhu et al. made impressive advances in 1988-1991 in modelling constant-amplitude laser fields on bulk water via NEMD (using either a sine- or cosine-wave variant of eqn (2) and (3), without the magnetic component), studying both structural and dynamical properties [130-132]. In 2004, Ohkubo et al. discussed subsequently NEMD of an aqueous solution of pyrimidine by modelling a laser field as a pure alternating electric field (cf. E in eqn (3)) [133], studying field-induced pyrimidine alignment. In 2002-2003, NEMD simulation was used to study time-dependent response of salts and ionic liquids to alternating pure electric fields, in the microwave frequency range by Tang et al. [134] and Petravic and Delhommelle [135]. The first reported case of application of an external EM field to NEMD was by Evans in 1991 [136], who studied magnetisation, finding a characteristic dependence thereof on frequency; it was suggested that this can be used in principle for (non-linear) spectroscopy for a range of materials. In that study [136], as well as [128], Evans discussed dispersion induced anisotropy in orientation in liquids due to non-resonant laser fields, whose high strength leads to non-linear response. In 2003‑2004, English and MacElroy reported microwave- and infrared-range EM fields applied in NEMD of heating in water (without any thermostat), [90] dipolar response and diffusion enhancement [89] and retarding crystallisation kinetics of clathrate hydrates [137].

2.5 Computational Approach

In this thesis, the general computational approach applied to investigate the effects of static (Chapter 3) and oscillating electric fields (Chapter 4) is described below. Specific information relevant to individual study are described in detail in the respective chapters. The protein model for all of our simulations was the apoC-II derived peptide apoC-II(60-70) (60MSTYTGIFTDQ70)[83]. Different starting conformations and arrangements of the peptide were investigated, detailed in the individual results chapters.

Explicit solvent MD simulations were conducted using the GROMACS 3.3 (www.gromacs.org) simulations package. The interatomic interactions were treated using the GROMOS force field parameter set 43A1 and the SPC water model. Long-range electrostatic interactions were evaluated using the Particle-Mesh Ewald (PME) method with a cutoff of 10 Å and a spacing of 1.2 Å for the FFT (fast Fourier transform) grid. The short-range neighbour list was cutoff at 10 Å. The peptide monomer was enclosed in a periodic cubic box sufficiently large to avoid significant cross-cell interactions with a minimum distance between the solute and the edges of the box of 12 Å. The simulation box was solvated with ~4080 SPC water molecules, corresponding to water density ~1.0 g/cm^3. The apoC-II(60-70) charge of -1 was compensated by adding Na+ counterion to ensure a neutral simulation cell. The MD simulations were conducted in the constant particle number, pressure, and temperature (NPT) ensemble with the target temperature and pressure maintained using the Berendsen [111] thermostat and barostat. The solvent and protein were coupled separately to a temperature bath at 300 K with a temperature coupling constant of 0.1 ps. Constant pressure of 1 bar was maintained uniformly in the system with a pressure-coupling constant of 1.0 ps. The fast degrees of freedom were neglected in our simulations and all-bond lengths were constrained using the LINCS algorithm [116], which enabled an integration time step of 2 fs to be used. The whole system was initially energy-minimised to remove steric clashes, using the steepest descent approach.

Here, the non-equilibrium molecular dynamics included an external electric or EM force. The theoretical background and application of the external electric and EM field in computational simulations are described in detail in the previous section and a recent review [7]. In summary, for the electric- (E) field simulations, the $f_{i,elec} = q_i E$ force is applied to each partial charge i, with charge value q_i. Newton's equation of motion then becomes $m_i \ddot{r}_i =$

$f_i + q_i E(t)$ where the force f_i is due to the classical molecular mechanics interatomic interactions (force field) between all the particles, and the electric-field vector $E(t)$ remains constant (i.e., formally a statically applied, time-independent field). For external EM field conditions, Newton's second law becomes $m_i \ddot{r}_i = f_i + q_i E(t) + q_i v_i \times B(t)$, where the force f_i is due to force field interactions between all the particles, and v_i is the velocity of the individual particle. The electric- (E) and magnetic- (B) field strengths are related by $\frac{E(t)}{B(t)} = c$, where c is the speed of light. The individual forces act along the mutually orthogonal *z*- and *y*- directions respectively, represented as $\mathbf{E}(t) = \mathbf{E}_{max} cos(\omega t)(0\mathbf{i} + 0\mathbf{j} + 1\mathbf{k})$ and $\mathbf{B}(t) = \mathbf{B}_{max} cos(\omega t)(0\mathbf{i} + 1\mathbf{j} + 0\mathbf{k})$, resulting in the plane of polarisation being in the *x*-*z* plane [89, 90].

Analysis of the trajectories, including Radius of gyration and N-C terminal distance, was performed with the Gromacs analysis tools, while visualisation of system geometries and interactions was achieved using Visual Molecular Dynamics (VMD) environment [138]. The total dipole moment of the protein was determined using $\mathbf{M}(t) = \sum_{i=1}^{N} q_i r_i(t)$, where q_i is the charge on atom *i*, r_i is the position of atom *i* with respect to the centre of mass of the protein, and N is the number of protein atoms. The autocorrelation function $C(t) = \langle \boldsymbol{M}(0) \cdot \boldsymbol{M}(t) \rangle / \langle \boldsymbol{M}^2(0) \rangle$ of the total dipole moment **M**(t) was used to provide insight into the dynamics and interrelation of the peptide dipole moment relative to the field over time.

Chapter 3
Effects of (static) electromagnetic fields on the structure and dynamics of apoC-II(60-70) peptide

3.1 Introduction

As described in detail in Chapter 1 the consequences of exposure of basic biological systems, including water, proteins, DNA, cell membranes, and entire cells, to EM radiation in the RF range have been a subject of intensive debate [1-8, 139]. It has become evident that the interaction between a molecular system and external EM field can give rise to a variety of unusual phenomena that can affect the cohesion and kinetics of matter over multiple length and time scales. Specifically to proteins, the mechanisms of non-thermal EM field effects are not well understood; however, it is believed that fields of specific frequency and strength can cause structural changes which can alter their conformation and, ultimately, their function [13, 14, 16-18, 140]. Changes in conformation can lead to misfolding and aggregation of proteins into insoluble aggregates or amyloid fibrils, which have been linked to debilitating diseases, such as atherosclerosis, Alzheimer's, Parkinson's, and others [2, 141]. Chapter 1 summarises the studies investigating EM field effects on proteins which have shown quite surprising and contradictory results. Some have suggested reversible changes in protein activity [5], while others have shown different field strengths and frequencies to cause opposite effects, from denaturation [3, 20, 140] to "freezing" of certain conformational states due to dipole alignment along the field direction [2, 3]. Therefore, these effects can contribute to the loss of native protein conformations and promote the development of amyloid fibrils [87, 141, 142]. In contrast, recent work has suggested that high-frequency RF fields are capable of destroying amyloid fibrils in Alzheimer's patients [143]. As stated in Chapter 1,

these contradicting results are indicative of a gap in our knowledge of RF biophysics and further studies may reveal novel applications of RF fields that could include treatment of diseases.

Computer modelling provides a unique opportunity to apply a systematic approach to better understand and quantify the immediate response mechanisms of biological molecules to EM radiation and monitor their dynamics at all-atom detail with femtosecond time step resolution, which is not currently accessible to experiments. In the present work, in contrast to most previous published papers in this area, wherein only electric-field (E) forces were taken into consideration, we include the explicit magnetic force (B) in a direction perpendicular to the electric field, which enables us to study the comprehensive effects of electromagnetic radiation. Although the electric-field strength is orders of magnitude greater than that of the magnetic component, the cumulative nonthermal effects of electric field versus EM fields on proteins have not been explored previously and present a computational challenge. The choice of field types investigated here (EM vs electric field) was motivated by the need to reveal systematically any role of the magnetic Lorentz-force contribution to the structure and dynamics of EM field-exposed biomolecules in physiologically relevant (aqueous) environments, in atomistic detail.

3.2 Computational Details

Non-equilibrium (electric-/EM field-applied) simulations were performed, starting from the wild-type apoC-II(60-70) structure (Figure 8) from different initial orientations with respect to the field direction and velocities (6 simulations per system/condition). For comparison and validation of our previous results [78, 144], equilibrium (zero-field, or ambient) simulations were also repeated starting from the same 6 starting orientations. Upon completion, the simulations were amalgamated in a single (ensemble) trajectory per field strength for analysis. The field strengths ranged from 0.7V/nm to $7x10^{-6}$ V/nm, and a total ~45 μs of data were collected for analysis. To compare and contrast the magnetic contributions, we mimic an application of a very-low frequency (long-wavelength) EM field, as opposed to an alternating electric field, and static electric field simulations of microsecond duration [7]. A "static" EMF over this simulation duration is equivalent to a formal EM field with frequency in the ~10-50 kHz range, in terms of cos ωt "decaying" from 1 to ~0.5 (or more) over the

individual simulation's duration. It should be noted that the larger of the field strengths applied in this study are several orders of magnitude larger than those applied typically, either experimentally or industrially. Previous simulation studies have shown it is necessary to use field strengths of the order of 1 V/nm to observe tangible effects within the limited time scales amenable to simulation [7, 14, 140]. With this in mind, this work provides a systematic comparison of electric versus EM field simulations in the intermediate to low strength range (i.e., 0.7 to $7\text{x}10^{-6}$ V/nm) over microsecond time scales, which has not been reported previously. However, the simulations at the very low field strengths $<7\text{x}10^{-4}$ V/nm showed no tangible differences vis-à-vis the zero-field case over the time scales considered and were not investigated further.

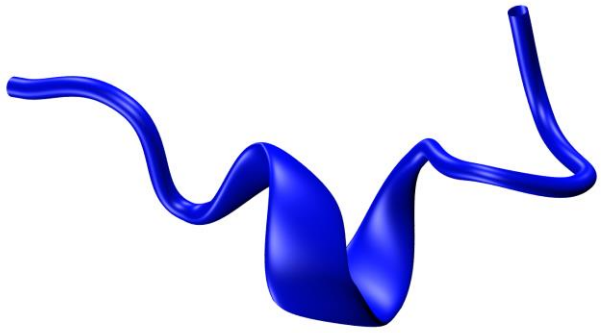

Figure 8: ApoC-II(60-70) wildtype peptide monomer (PDB code 1SOH)

The evolution of each system was monitored and most frequently sampled conformations were classified using the single-linkage clustering algorithm [145]. In this "bottom-up" geometric clustering approach, a structure is assigned to a cluster when its root mean square deviation (RMSD) is below a predefined cutoff. The appropriate cut-off value was identified by repeating the clustering analysis for a range of RMSD values in the ambient (zero-field) simulations until the top 3 most populated clusters comprised over 50% of structures used for the clustering analysis. An all-atom RMSD cutoff of 0.18 nm was found appropriate and was applied to all ensemble trajectories to identify the structural differences between the ambient and in-field simulations. Visualisation of system geometries, interactions, and dipole orientation was achieved using the Visual Molecular Dynamics (VMD) environment [138]. The total dipole moment of the protein was determined as $\mathrm{M}(t) = \sum_{i=1}^{\mathrm{N}} q_i \mathrm{r}_i(t)$, where q_i is the charge on atom i, r_i is the position of atom i with respect to the centre of mass of the protein, and N is the number of protein atoms. The autocorrelation function $C(t) =$

$\langle \mathrm{M}(0) \cdot \mathrm{M}(t) \rangle / \langle \mathrm{M}^2(0) \rangle$ of the total dipole moment M was used to provide insight into the dynamics and interrelation of the peptide dipole moment relative to the field intensity over time.

3.3 Results and Discussion

Extensive MD simulations in explicit solvent were performed to explore the structural behaviour and dynamics of the amyloidogenic apoC-II(60-70) peptide in ambient and applied external-field conditions, including EM field and electric field of different strengths. The water structure and mechanisms of interactions for each field condition were also examined.

Clustering analysis using the linkage technique was performed to identify the preferred structures for the most frequently sampled conformations for each system. A structure was assigned when its all-atom RMSD was less than 0.18nm relative to all members of that cluster. The total number of clusters obtained and the population of the most frequently sampled structure for each field strength are shown in Figure 9.

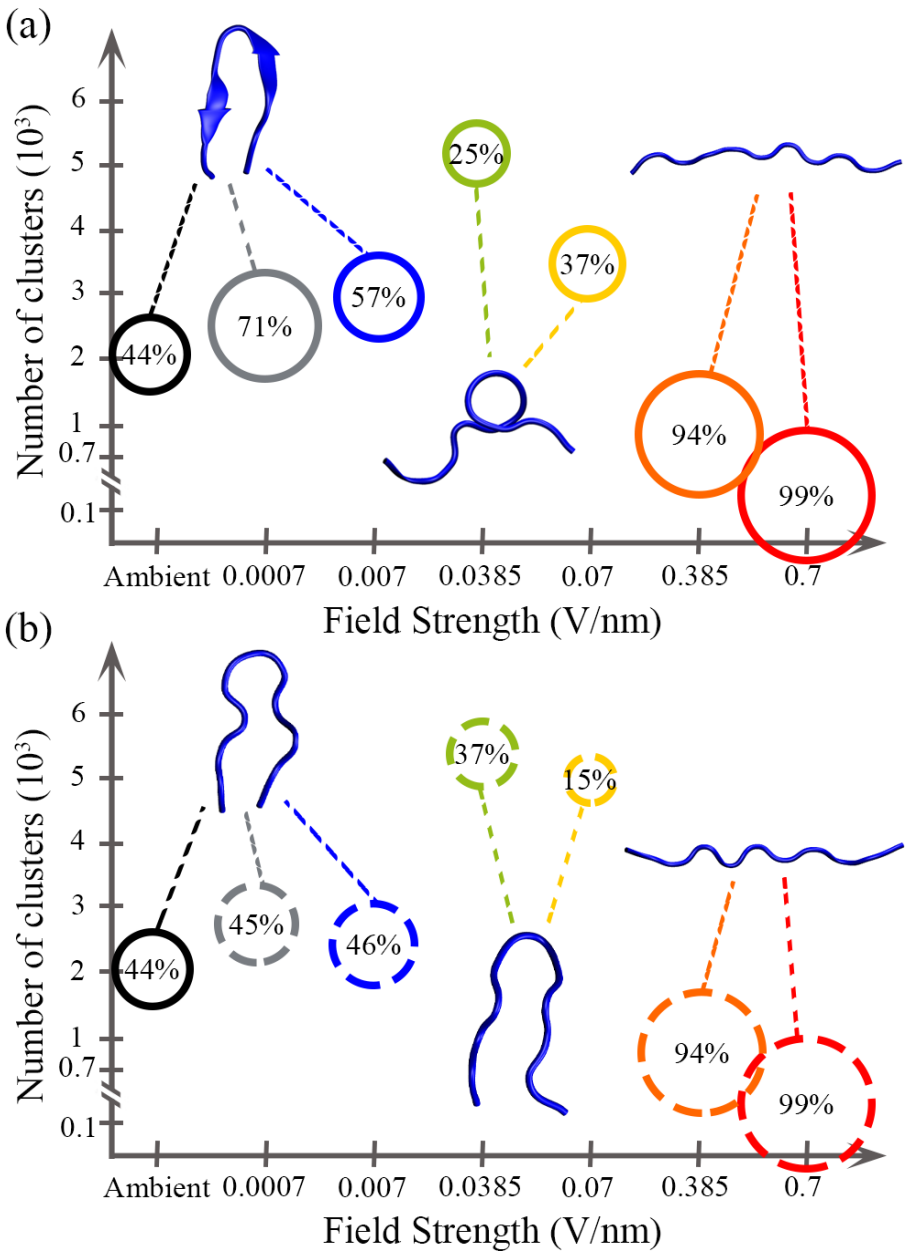

Figure 9: Schematic diagram showing the total number of clusters (represented by the centre of each circle relative to the y-axis) sampled at different field strengths for the (a) EM field and (b) electric field simulations. Each field strength (V/nm) is represented by colour; 0.0007 (grey), 0.007 (blue), 0.04 (green), 0.07 (yellow), 0.4 (orange), and 0.7 V/nm (red). The ambient (field-free) MD results are also shown for comparison (black). The circle size (to scale) represents the population of the most persistent cluster. Representative structures of the most populated clusters are shown as insets.

The cluster analysis of the ambient (field-free) ensemble trajectory identified three highly sampled clusters (with populations >10%), with the most-populated clusters comprising 44% of all MD-sampled structures. Despite the more substantial sampling than previously reported [78, 144], the typical representative apoC-II(60-70) structure of the highest populated cluster was a β-hairpin conformation, deemed as an intermediate state for fibril formation in our earlier work [144]. Cluster analysis results from the EM field and electric field simulations exhibited similar trends, in terms of the total number of clusters explored per field strength, in spite of some differences in structure and cluster populations. The simulations of low field strengths (<0.007 V/nm) showed clusters with predominantly β-hairpin conformations, although the EM field simulations produced more populated clusters (71% and 57% for 0.0007 and 0.007 V/nm, respectively), compared to the electric field simulations (45% and 46%, for the same field strengths), which had similar populations to the ambient system.

This suggests that the EM field may possess the ability to stabilise (or "trap") the peptide in certain conformations; however, rationalisation of this observation requires further insight into the mechanisms of EM field interactions with the peptide (discussed later). As the field strength increased, the effects of the field on the peptide conformation became more apparent. The peptide became more dynamic and sampled a large number of clusters, where the most populated clusters compromised 25% (0.04 V/nm) and 37% (0.07 V/nm) of structures from the EM field simulations, and 27% (0.04 V/nm) and 15% (0.07 V/nm) from the electric field simulations. In this medium field strength range (0.04-0.07 V/nm), the most populated clusters from the EM field simulations consisted predominantly of twisted conformations, wherein the peptide retained the loop region at Gly65, and the N- and C-termini are separated, while the electric field simulations exhibited structures with β-hairpin-like conformations. Such increased peptide mobility and conformations devoid of β-hairpin elements were determined previously to correspond to typical fibril-inhibiting characteristics of apoC-II peptide [78, 144]. The difference in cluster populations and structures sampled across all EM field strengths and compared to electric field simulations suggests that the magnetic contribution in EM field simulations may be small, but non-negligible; however, the observed effects arising as a consequence of limited conformational sampling can also not be disregarded. As expected, the higher-strength EM and electric field (>0.3 V/nm) had the most significant effect on the peptide conformations. The peptide adopted mostly extended structures, for which the whole peptide dipole aligned along the applied field direction for over 94% of the MD trajectory. Similar dipolar alignment and enhanced conformation-

sampling kinetics have been observed for alanine peptides, and clusters thereof, as a function of EM field strength [146].

To obtain further insight into the conformational landscape induced by each field type and strength, a free-energy map (FEM) of the peptide's radius of gyration (R_g) was determined, as a function of N-C terminal distance. The free energy was calculated using $-k_B T \log(N_i)$, where k_B is Boltzmann's constant, T is temperature, and N_i is the total number of structures contained within a cluster i of the two properties. The most frequently visited regions at each field strength were identified by calculating the average of each property from the structures contained within the most populated cluster of each EM/electric field ensemble simulation. The ambient (zero-field) simulations exhibited a single energy well populated by structures predominantly in a β-hairpin conformation, with an average terminal distance of 0.41 ± 0.06 nm and Rg of 0.61 ± 0.02 nm, as seen from the clustering analysis. The inherent flexibility of the peptide is demonstrated by the evident smearing of the FEM showing regions of higher energy, i.e., less-populated states of larger Rg and terminal separation. In contrast, the applied-field simulations identified two low-energy valleys connected by less populated transitions states. The high-field strengths (>0.3 V/nm) induced elongation of the peptide conformation, where both EM and electric field simulations sampled similar regions on the FEM with ~3.5 nm average N-C terminal distance separation and ~1.09 nm, average Rg. In the medium-strength field range (0.04-0.07 V/nm), we observed diverse conformations, which provide the transitional pathway between the elongated (high-field) and compact (low-field) peptide states. Here, we also observe some differences between the EM- and electric field-sampled structures. Specifically, the electric field simulations exhibit a broader transition pathway between the two low energy states, indicating external electric fields of 0.04-0.07 V/nm strength induce significant structural dynamics in the apoC-II(60-70) peptide, preventing it from stabilising in a particular conformation, as evidenced by the large number of clusters obtained in our cluster analysis (vide supra). The broad landscape sampled for these field strengths, together with the contributions of individual simulations to the overall FEM. In contrast, the EM field simulations exhibited narrower transitional pathways, confirming our initial observation that the applied EM field was able to stabilise, or trap, certain conformations of the peptide. This is demonstrated here by the highly populated cluster (37%) observed in the 0.07 V/nm EM field that features structures with average N-C terminal separation of 1.86 ± 0.15 nm, compared to electric field simulations where the most significant cluster had only 15% and structures with terminal separations of 0.64 ± 0.13 nm.

The distinct structural preference induced by the 0.07 V/nm EM field simulations is demonstrated by the presence of two "hot spots" along the transition pathway (~3 nm N-C distance/~0.97 nm Rg and ~1.8 nm N-C distance/~0.61 nm Rg). At the low field strengths (<0.007 V/nm), the peptide sampled the same region on the FEM as in the ambient simulations, populated by β-hairpin structures with average terminal separations of ~0.45 ± 0.08 nm and 0.44 ± 0.07 for the EM and electric field simulations, respectively. Similar to the medium field strength, the EM field simulations exhibited significantly more stable clusters compared to the electric field and ambient simulations, although with similar structural features.

3.3.1 Aromatic Angle Distribution

Hydrophobic interactions, especially those between aromatic side-chains, have been shown to play an important role in the structure and function of proteins, and, more recently, in the formation and stabilisation of amyloid fibrils. In our previous work, we have established that the two aromatic rings (Tyr63 and Phe67) present in the apoC-II(60-70) peptide play a crucial role in the peptide's mechanism of aggregation [144]. Importantly, we found that there are distinct differences in the aromatic side-chain orientations between fibril-forming and fibril-inhibiting states of the peptide. We identified that under fibril-inhibiting conditions, the aromatic rings adopt conformations where Tyr63 and Phe67Ile are on the same side of apoC-II(60-70) peptide, whereas structures obtained under fibril-favouring conditions have aromatic rings on the opposing sides, thus enabling the π-π stacking interactions between the neighbouring peptides leading to the fibril growth [78, 82, 144]. Here, the relative orientations Tyr63 and Phe67 in apoC-II(60-70) under EM and electric field exposure were determined by calculating the average angle between the Cα-Cγ vector of Tyr63 and the Cα-Cγ vector of Phe67.

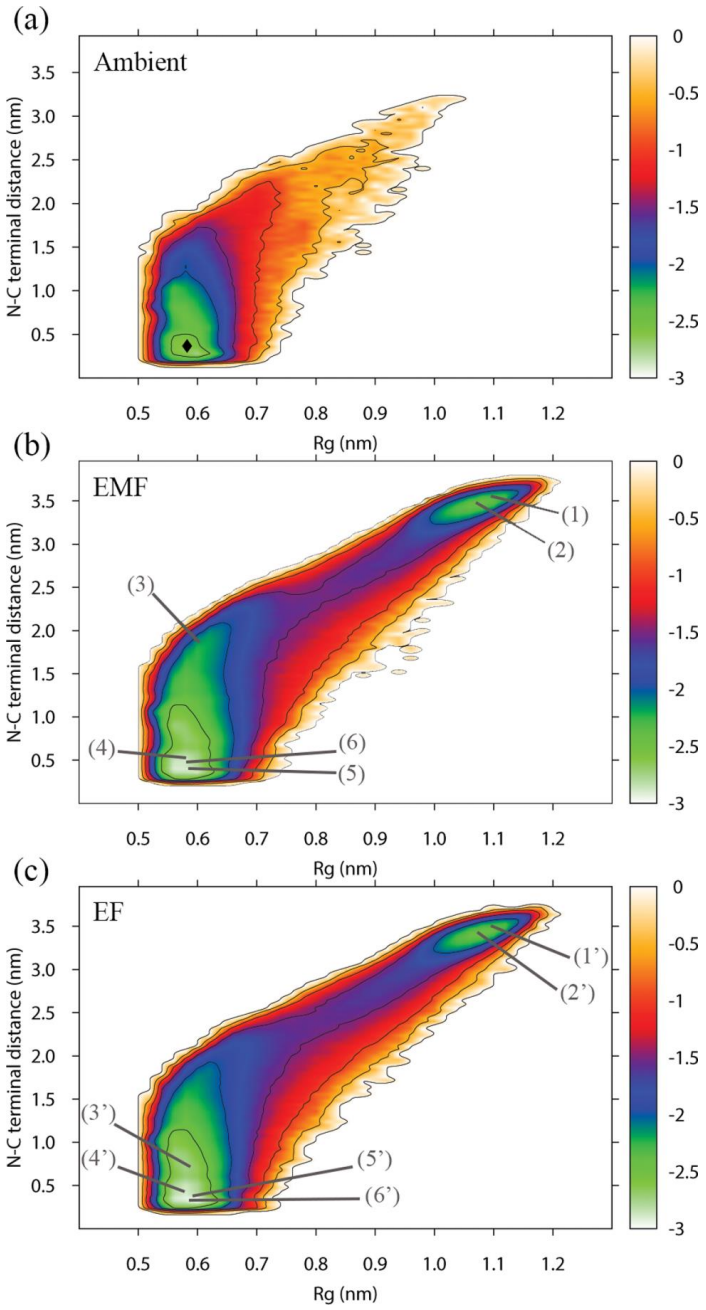

Figure 10: Free energy map (FEM) as a function of the radius of gyration (x-axis) and N-C terminal distance (y-axis) of the apoC-II(60-70) peptide under (a) ambient, (b) EM, and (c) electric field conditions. The location of the most-populated cluster on the FEM from the ambient simulation is labelled with symbol (⇧). The most-populated cluster from each simulation of varying field strength is identified by a number: (1) 0.7 V/nm, (2) 0.385 V/nm, (3) 0.07 V/nm, (4) 0.0385 V/nm, (5) 0.007 V/nm, (6) 0.0007 V/nm, where the EM field simulations are labelled with unprimed and electric field simulations with primed numbers.

Figure 10 shows the percentage of sampled structures with respect to the relative orientation of the aromatic rings of the peptide in the two most-populated clusters identified in each simulation. A total of 40 bins were used over the range 0°-180°. Angles <90° indicate that both rings are on one side of the peptide, while angles >90° indicate that the rings are on the opposite sides. The results from the high-strength applied-field simulations (>0.3 V/nm) showed structures with a broad distribution of the angles between the aromatic pairs, as expected due to the elongated conformations sampled at this level of exposure. The 0.07 V/nm trajectories showed peptide preference for angles between the aromatic rings of less than 90°, with peaks seen at 30° and 50° for the EM and electric field simulations, respectively. This suggests that apoC-II(60-70) adopts fibril-inhibiting structures at this "intermediate" field range strength. As the applied field strength approaches the lower field range, there is an evident shift in the in the aromatic-angle orientation preference to the opposite peptide faces. The results for the most populated cluster showed that in the EM and electric field and <0.04 V/nm strengths, apoC-II(60-70) prefers a relative aromatic ring orientation angles larger than 90°, with peaks seen at ~140°, despite the differences in structural stability between the different field types and strengths. This behaviour is similar to the structures sampled in ambient conditions and suggests that low-strength fields induce fibril-forming characteristics of the apoC-II(60-70) peptide. The diverse aromatic angles observed from the EM field compared to the electric field simulations suggest that although the two different fields cause the peptide to adopt similar structures, the EM field has a more evident effect on the orientation and dynamics of the aromatic residues. Figure 11 also shows a shift in aromatic angle preference between the highest and second most populated cluster for most field strengths except the EM field of 0.07 V/nm, which retained the orientation angles at <90° and 0.007 V/nm, which showed more frequent occurrence of structures with aromatic side-chains on opposite face of the peptide. This highlights further that the EM field simulations sampled two different conformational energy states, confirming the clustering and FEM analyses discussed previously.

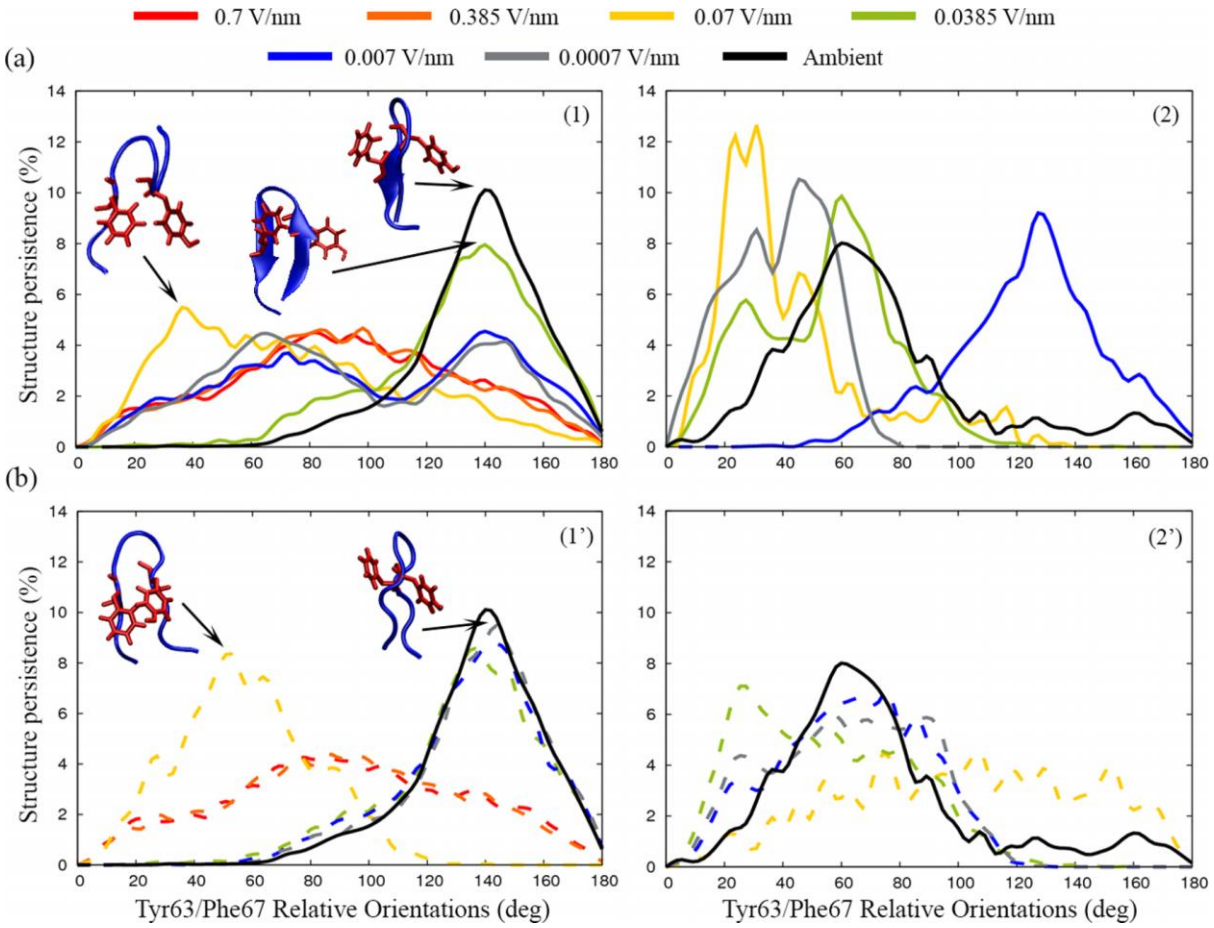

Figure 11: Distribution of aromatic-ring orientation in apoC-II(60-70) peptide under (a) EM field and (b) electric field exposure. Histograms of the relative aromatic ring orientation (x-axis) of residues Tyr63 and Phe67 in two most populated clusters (labelled as 1 and 2) for each field strength (y-axis). Typical structures illustrating the most frequently sampled relative ring orientations of apoC-II peptide are represented as insets.

3.3.2 Peptide and water dipole orientation

The applied EM and electric field external fields have a direct effect on the molecule's dipole moment, which contributes to the transitional and rotational motion exhibited by the protein and water. The dipole moment of the starting (native) structure of apoC-II(60-70) peptide is ~129 D. In the presence of high field strengths (0.7 V/nm), the resultant elongated conformation of the peptide exhibited a dipole moment of ~254 D. In contrast, a decrease in the field strength resulted in a reduction of the dipole moment as the peptide was able to adopt the inherent β-hairpin-like structures. At 0.0007 V/nm, the β-hairpin conformations of apoC-II(60-70) had a dipole moment of ~53 D, similar to the dipole moment of ~56 D

calculated under ambient (zero-field) conditions. Figure 12 shows the peptide dipole autocorrelation function, as well as the water dipole-moment order parameters (with respect to the z-axis, along which the electric-field component is applied), providing insight into the dynamics and interrelation of the peptide/water dipole moment relative to the field strength over time. Peptide- and water-dipole orientations in the low- and high-strength fields are also illustrated by representative snapshots from the simulations. The results of both field types demonstrate that the peptide dipole moment is highly correlated for high field strengths (>0.3 V/nm), revealing the persistent alignment of the peptide dipole with the applied field. As the field strength is decreased to ~0.03 V/nm, there is also a gradual decrease in the dipole correlation. The low-field strengths (<0.007 V/nm) exhibit no correlation of the peptide dipole moment, in line with the field-free (ambient) simulations where the field had no effect on the peptide dipole moment. Similarly, the water dipole experiences a reduction in order and alignment as the field strength is reduced, and at the extremely low field strengths it adopts the characteristics of bulk water. This is in line with previous observations of EM field effects on water molecules in the immediate environment (solvation layer) of hen egg white lysozyme [140], as well as for studies of bulk water [89]. There was no noticeable difference in the peptide and water dipole moment structuring between the applied EM and electric field. Overall, the dipole analysis showed that field strengths higher than 0.007 V/nm are required for the system to experience any noticeable effects on dipole orientations.

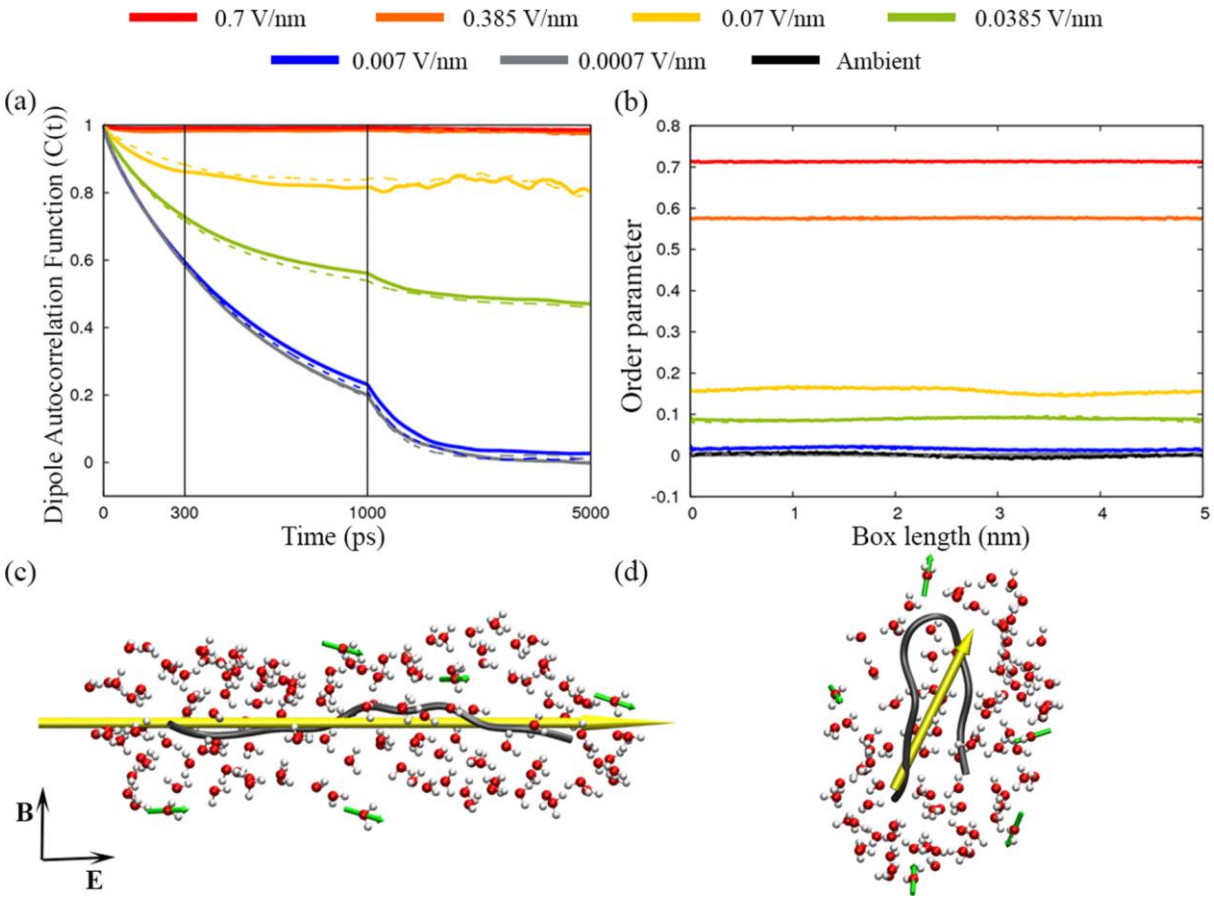

Figure 12: Peptide dipole autocorrelation function with water (a) and water dipole-moment order parameter (b) shown for EM and electric field simulations (solid vs. dotted lines, respectively). Representative structures are depicted for the peptide and the hydration layers of the systems exposed to (c) 0.7 V/nm and (d) 0.0007 V/nm fields. The peptide and water dipole moments are shown as yellow and green arrows, respectively. The direction of the applied fields E (electric) and B (magnetic) is shown by arrows.

3.3.3 Peptide-water interactions

It is also important to understand the peptide interactions with water when exposed to different field types and strengths. Peptide-water interactions and structuring of water around the peptide play a significant role in peptide's conformation, dynamics, and, ultimately, function. Specific interactions between the apoC-II(60-70) peptide and solvent were evaluated by calculating the radial distribution functions (RDFs) over the equilibrium stage of the simulations (cf. Figure 13). The RDFs between apoC-II peptide and water exhibit three distinct peaks: the first two at ~0.18 and ~0.30 nm indicated hydrogen bonding between water and the peptide, leading to formation of the first hydration shell, and the second at ~0.45 nm, suggesting a second hydration shell. The sharp water-peptide peaks indicate a persistent structuring of water around the peptide, with a decrease in water packing as the field strength decreases. This suggests that the peptide is more solvated at the higher field strengths, in the sense of a greater local density of water in the immediate solvation layers. Indeed, this effect is much influenced by its then-preferred (dipole-) extended conformations, causing the exposure of all residues, including hydrophobic residues. In contrast, the low-strength fields allow the peptide to fold, or "coil", into its inherent β-hairpin conformation, where it becomes less solvent exposed. There are no obvious differences between the peptide-water RDF profiles from the EM and electric field simulations except for at 0.07 V/nm, where we observe a minor disparity. This suggests that the contributions of the magnetic forces in the EM field simulation have a negligible effect on the local structuring of water in the solvation layer.

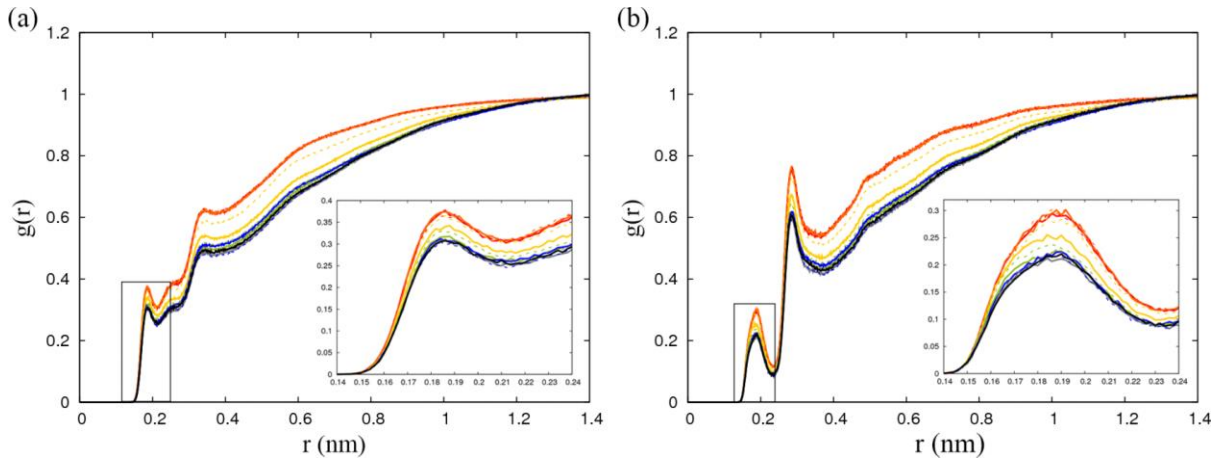

Figure 13: Peptide-water interactions represented by radial distribution functions of (a) peptide (NHO)-water (H) and (b) peptide (NHO)-water (O). The RDFs from EM field simulations are shown in bold lines, and electric field simulations in dashed lines. The line colour is representative of the field strength: 0.7 V/nm (red), 0.385 V/nm (orange), 0.07 V/nm (yellow), 0.0385 V/nm (green), 0.007 V/nm (purple), 0.0007 V/nm (grey), and ambient (black).

3.4 Conclusion

In this Chapter we employed all-atom non-equilibrium dynamics simulations to study the response mechanisms of the amyloidogenic apoC-II(60-70) peptide in aqueous solution to external electromagnetic and electric fields of different strengths. Our results showed that the peptide (and water) behaviour is strongly influenced by the field strength. High field strengths (>0.04 V/nm) caused the peptide to elongate and be devoid of its inherent β-hairpin structure, which is attributable overwhelmingly to the dipole-alignment effects of the electric-field component. In the "intermediate" field strength range, between 0.04 and 0.07 V/nm, the simulations showed intriguing behaviour by the apoC-II(60-70) peptide, where some differences between the EM- and electric field-induced structures became apparent. The peptide was significantly more dynamic in this field range, and in the EM field simulations, in particular, adopted conformational characteristics typical for its fibril-inhibiting behaviour, in that well-separated N- and C-termini are prominent, together with the aromatic-ring location's preference for the same face of the peptide. The simulations also revealed differences between the EM and electric field effects on the peptide free-energy landscape, especially whilst transitioning between respective high- and low-strength fields. Specifically, the EM field was able to constrain or "trap" the peptide in a twisted (non-β-hairpin like) conformation and limit the available conformational space, in contrast to the electric field simulations where the peptide was found to be more dynamic and adopted predominantly β-hairpin-like structures. The low-strength simulations (<0.007 V/nm) produced stable β-hairpin peptide conformations, similar to those seen in ambient conditions. The aromatic Tyr63/Phe67 pair showed preference for the opposite faces of the peptide, suggesting a fibril-forming peptide capacity at such conditions. It has to be noted that despite our extensive simulation times and relatively thorough sampling, it remains an open question whether the nuances in the peptide's conformational preferences observed between the electric and EM field are indeed caused by the additional magnetic force or are caused by the finite nature of the simulations, at least until it becomes possible to identify such atomic-level quirks experimentally. Our theoretical analysis of the peptide and water dipole moments, including the structuring of water around the peptide as a function of the field strength, demonstrated that at least a 0.007 V/nm field is required for any field effects to be observed. Most importantly, our study suggests that EM field could be considered for designing alternative treatments of amyloid diseases due to its inhibiting effect on the amyloidogenic peptide conformations for the intermediate strength, whilst the very high- and low-field strengths

stabilising amyloid favourable peptide conformations could be employed for engineering well-ordered peptide assemblies for other applications.

Chapter 4
Conformational response of an amyloidogenic peptide to oscillating electromagnetic fields: Effects of the field frequency and strength

4.1 Introduction

While studies of static electric field effects can be quite useful, as demonstrated in Chapter 3, fields emitted by the ubiquitous radio frequency EM devices are oscillating with continuously alternating strength and a frequency specific sinusoidal modulation. This requires a multi-parametric approach to accurately elucidate the effects of EM field exposure from RF devices. The effects of oscillating EM and electric fields on biological systems and responses have been previously investigated using computer simulations, although at higher field strengths and shorter timescales than those presented here. For example, Budi et al. studied the influences of oscillating electric fields of varying frequency (1.225, 2.45 and 4.9 GHz) and strength (0.01 to 1.0 V/nm) on the structure of the insulin chain B peptide and complete insulin monomer [2, 3, 96, 147]. Their results showed that a 2.45 GHz oscillating field can cause protein denaturation at lower field strengths compared to static fields of the same effective strength, where the latter were seen to have a stabilising effect on the helical regions of the protein. Interestingly, the low strength fields of the lower 1.225 GHz and higher 4.9 GHz frequencies induced similar behaviour in the peptide to that of the oscillating field of 2.45 GHz frequency. This suggested that the oscillatory nature of the electric field has a more destabilising effect on the protein structure relative to the static fields of the same effective strength. At higher frequencies, the high rate of the field direction change was suggested to

accelerate the destabilization of the peptide structure, as the peptide was exposed to more instantaneous changes of the electric field strengths. Simulations on the complete insulin monomer [3], showed increased stability under ambient and thermal conditions due to the stabilising effect of chain-A compared to the isolated chain B. The exposure to an oscillating field resulted in reduced conformational change of the monomer as all three helical regions tried to align with respect to the applied field which was energetically more demanding, and the protein response was ultimately determined by the applied frequency. The 1.225 and 2.45 GHz fields were able to induce the loss of secondary structure, while the 4.9 GHz field had no effect, possibly due to the oscillations of the field being too rapid for the protein to be able to follow and result in stable conformational changes.

In a similar study, English et al. examined the effects of EM fields of high strength (1.0-5.0 V/nm) and frequency (50-500 GHz) on the structure and dynamics of hen egg-white lysozyme (HEWL) protein and compared it to protein behaviour at elevated (400 and 500 K) temperatures conditions [14]. They observed the application of fields greater than 5.0 V/nm_{rms} led to more extensive protein unfolding than the very high temperature of 500 K. The authors also investigated the effects of microwave frequencies (2.45 GHz) and lower field strengths (0.1 to 1.5 V/nm_{rms}) on the same protein [15]. Under these conditions, they noted significant non-thermal effects occurring at field strengths above 0.1 V/nm, which included marked changes in the protein's secondary structure relative to ambient conditions. The majority of structural changes were found to take place instantaneously (within the first 0.2 ns of field exposure), due to the rearrangement of hydrogen bonds, while charged residues were found to undergo more localised motions, especially in solvent exposed regions that were adjacent to the active site, leading to greater hydrogen bond disruption. A separate study also looked at the effects of static [148] and oscillating fields [149] on the chignolin peptide to investigate the effects of static fields of 0.1 and 1.0 V/nm field strengths, and oscillating fields of 0.30 and 111 GHz at 1.0 V/nm. Low frequency, or static electric fields of high strength were capable of distorting the peptide's structure, while high frequency fields did not induce conformational changes. It is evident from the presented works that the nature of the interactions between oscillating fields and proteins is strongly dependent on the protein sequence, field conditions and simulation time scales. In order to gain further insight into the protein response to EM radiation it is necessary to systematically examine the behaviour of proteins and their solution environment under various EM field exposure conditions in atomistic detail while benchmarking it to the protein behaviour under ambient conditions.

Here, we extend our previous work on static EM field effects [83] into investigating the role of frequencies in the range of radio-frequency (1.0 and 2.5 GHz) and high frequency (5.0 GHz) commensurate with the upcoming rollout of 5G telecommunication networks, on the apoC-II(60-70) peptide conformation and dynamics for which we have accumulated ample benchmarking data for comparison [52, 60, 76-78, 82, 83]. Using these data and following from our recent study of the static field effects [83] on this peptide, we present a systematic study of the EM frequency effects on the structure, dynamics of the amyloidogenic apoC-II(60-70).

4.2 Computational Details

In this chapter we used two different starting structures of the apoC-II(60-70) peptide (wild-type and ß-hairpin) to alleviate any conformational "bias" of the initial structure and increase the conformational sampling (Figure 14). The native conformation of monomeric apoC-II(60-70) (^{60}MSTYTGIFTDQ^{70}) was extracted from the NMR structure of human apoC-II (PDB code 1SOH), while the hairpin conformation was taken from stable clusters formed in static field simulations presented in Chapter 3, also deemed as most stable solution structure under ambient conditions [83].

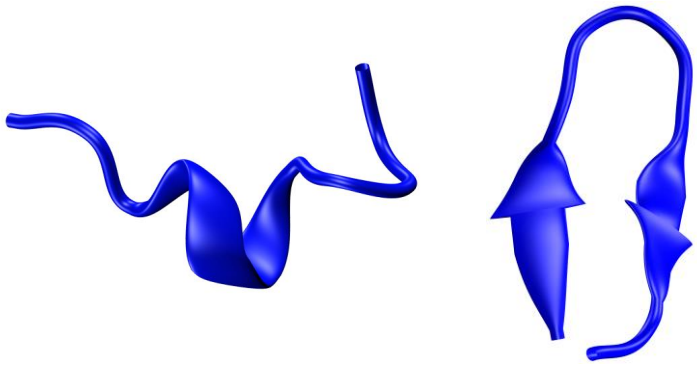

Figure 14: ApoC-II(60-70) peptide monomers, wildtype (left), and hairpin (right) conformations.

Non-equilibrium simulations were performed from the two different starting structures (wild-type and β-hairpin) and two different starting orientations to reduce any initial structural bias and enhance the conformational sampling. Field frequencies of 1.0, 2.5 and 5 GHz were simulated at different field strengths. The effective RMS field strengths investigated, $E_{RMS} = (\frac{E_{max}}{\sqrt{2}})$, were commensurate to those applied in our recent study on static fields [83],

with the following peak (and respective RMS) field strengths; 0.9899 V/nm (0.7 V/nm_{rms}), 0.09899 V/nm (0.07 V/nm_{rms}), 0.0544 V/nm (0.0385 V/nm_{rms}), 0.009899 V/nm (0.007 V/nm_{rms}), 0.0009899 V/nm (0.0007 V/nm_{rms}). Each structure/orientation system was simulated for 200 ns (except for the 0.7 V/nm_{rms} simulations), resulting in a total of 400 ns per structure for each field strength/frequency combination. The individual structure and field condition simulation times are listed in Table 2. Close analysis of the individual structure trajectories showed that the simulations had equilibrated within 150 ns. The last 50 ns of simulation were taken from each equilibrated trajectory (for each field strength/frequency combination) and were amalgamated into a single (ensemble) trajectory of 200 ns for analysis. For comparison to the ambient and static field conditions, the same analysis approach was repeated on the previously collected data [83].

Table 2: Simulation times (ns) of ApoC-II(60-70) under oscillating fields at various field strengths

	1.0 GHz	2.5 GHz	5.0 GHz
0.0007 V/nm	2750	2750	800
0.007 V/nm	800	800	800
0.0385 V/nm	800	800	800
0.07 V/nm	800	800	800
0.7 V/nm	600	200	200

The evolution of each system was monitored and the most frequently sampled conformations were classified using the GROMOS clustering algorithm [150]. The GROMOS clustering method produces a series of non-overlapping clusters, where the structure with the highest number of neighbours is taken as the centre of a cluster, which is formed together with its neighbours to create the (first) cluster, and then removed from the pool of structures. The process is repeated for all structures in the trajectories. Structures were assigned to a cluster by calculating the all-atom RMSD with a cut-off of 0.22 nm. The appropriate cut-off was determined by performing clustering analysis using different cut-offs initially on the 0.0007 V/nm/1.0 GHz ensemble trajectory, until the top 3 clusters comprised over 50% of the simulated structures. Radius of gyration and N-C terminal distance analysis was performed with the Gromacs analysis tools, while visualisation of system geometries and interactions

was achieved using Visual Molecular Dynamics (VMD) environment. The total dipole moment of the protein was determined using $\mathbf{M}(t) = \sum_{i=1}^{N} q_i r_i(t)$, where q_i is the charge on atom i, r_i is the position of atom i with respect to the centre of mass of the protein, and N is the number of protein atoms. The autocorrelation function $C(t) = \langle \boldsymbol{M}(0) \cdot \boldsymbol{M}(t) \rangle / \langle \boldsymbol{M}^2(0) \rangle$ of the total dipole moment **M**(t) was used to provide insight into the dynamics and interrelation of the peptide dipole moment relative to the field over time.

4.3 Results

Extensive all-atom MD simulations were performed to investigate the effect of oscillating EM fields of different field frequencies and strengths on the conformational response mechanisms of the amyloidogenic peptide apoC-II(60-70). The effects of the EM field parameters on the peptide secondary structure, size, relative residue orientation, solvent structure and dynamics as well as the molecular mechanisms driving these responses were investigated.

Peptide structure and dynamics

The most stable (frequently sampled) conformations of each ensemble trajectory were determined by clustering analysis using the GROMOS method with an all-atom RMSD cut-off of 0.22 nm. The total number of clusters sampled along with the representative structure and population of the most favourable conformation are shown as insets in Figure 15. Clustering analysis was also performed on the previously reported ambient and static field simulations [83] using the same GROMOS clustering method for comparison. The results showed substantial structural and dynamic differences in the peptide under the static and oscillating field conditions, in line with other theoretical studies [2], [149].

The most immediate influence of the frequency was observed in the simulations at high field strength (0.7 V/nm_{rms}). There was ~15-28-fold increase in the total number of clusters sampled as the field frequency increased from 1 to 5 GHz, albeit the clusters had very low population. The peptide was seen to continuously alternate between extended and collapsed (β-hairpin-like) conformations due to the strong peptide dipole alignment along the field

direction at the peak strengths. This suggests that the peptide experienced quasi-instantaneous response to the highest strength oscillating EM field for the entire studied frequency range which culminated in the increased peptide dynamics relative to its native behaviour (see movie in Supporting Information).

The simulations at intermediate field strengths (0.07-0.0385 V/nm_{rms}) exhibited an overall lower number of total clusters sampled at all frequencies, compared to the static field simulations with the same effective field strength. The low to intermediate frequency (1.0 to 2.5 GHz) simulations showed more highly populated (stable) clusters of structures with similar β-hairpin-like conformation, relative to the lower strength static field and ambient simulations. This suggests the EM fields with intermediate field strengths and RF frequencies have the ability to stabilise (or "kinetically trap") the peptide in specific conformations. This is most evident in the 2.5 GHz simulations, suggesting that this combination of the EM field parameters has the field strength sufficient to induce conformational changes but at the same time it allows adequate time for the peptide to adopt a more thermodynamically stable conformation due to the reversal of the field direction. This is in contrast to the static field results where the continuous and unidirectional force caused the peptide to adopt a thermodynamically unfavourable non-native conformation. The high 5.0 GHz frequency simulations at the intermediate field strengths exhibited similar clustering results to the ambient and static field simulations of lower (< 0.007 V/nm_{rms}) field strength.

Interestingly, at the low field strength (< 0.007 V/nm_{rms}) the peptide produced the lowest total number of clusters sampled across the 1.0-2.5 GHz frequencies, compared to the static field and ambient simulations. This suggests that these RF frequencies combined with the low field strength appear to have the ability to trap the peptide in specific conformations, resulting in reduced peptide dynamics. Here, the field strengths are seemingly insufficient to have a significant effect on changing the peptide conformation, while the relatively (un)frequent change in field direction has a restraining (trapping) effect on the peptide dynamics. A more accurate rationalisation of this observation requires further insight into the mechanisms of EM field interactions with the peptide (discussed later). In contrast, the 5.0 GHz simulations revealed native-like sampling statistics (clustering) of the peptide structures similar to the ambient and low strength static field conditions. This suggests that the high oscillation frequency EM field does not appear to affect the inherent peptide dynamics.

While clustering analysis provides an overall insight into the relative stability and dynamics of the peptides, a more detailed structural analysis is needed to determine the effect of EM frequency on the conformational landscape of the peptide. To achieve that the free energy maps (FEM) of the peptide's radius of gyration (R_g) as a function of the N-C terminal distance were constructed (Figure 15).

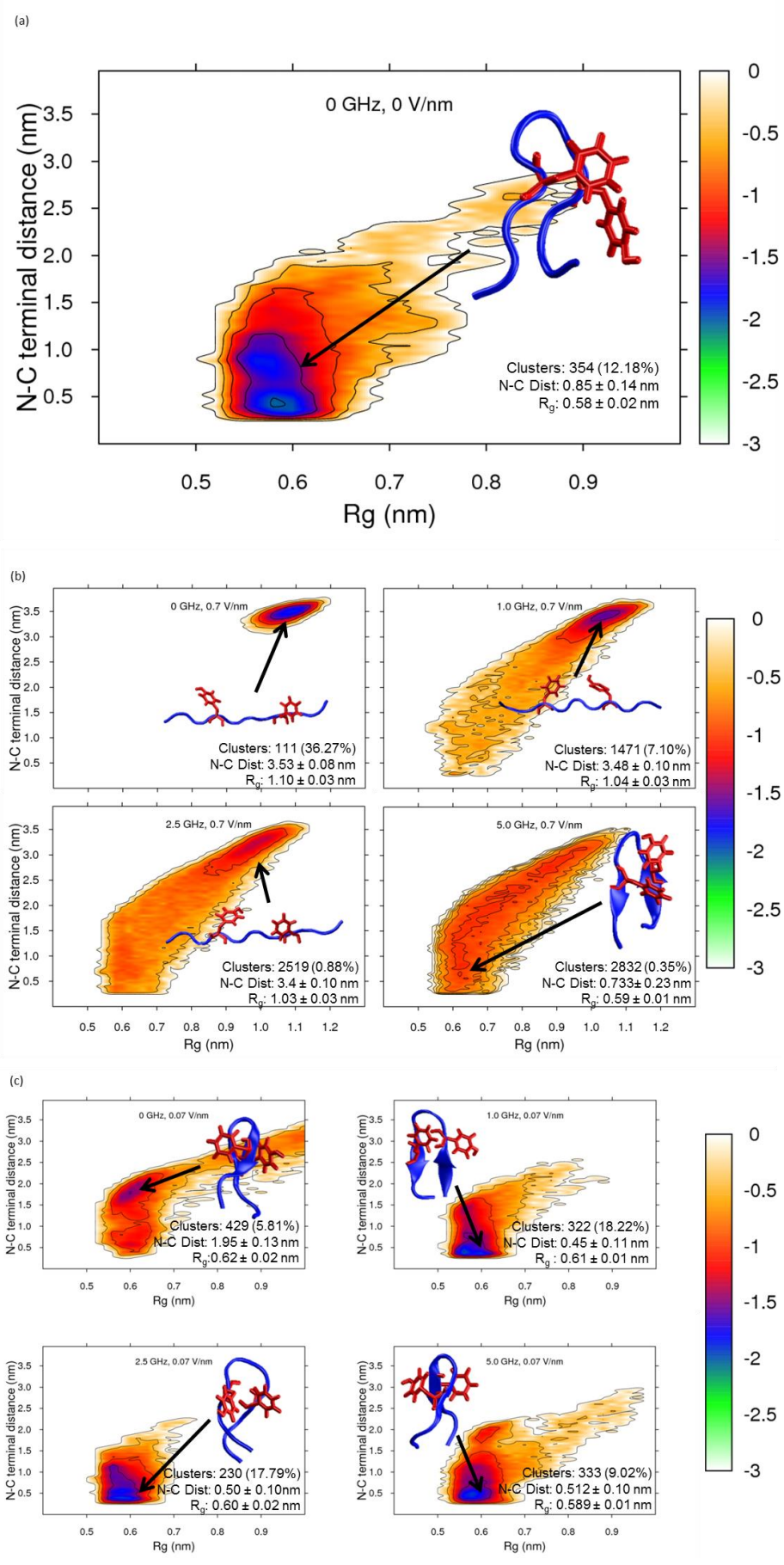
(a)
0 GHz, 0 V/nm
N-C terminal distance (nm)
Rg (nm)
Clusters: 354 (12.18%)
N-C Dist: 0.85 ± 0.14 nm
Rg: 0.58 ± 0.02 nm
(b)
0 GHz, 0.7 V/nm
Clusters: 111 (36.27%)
N-C Dist: 3.53 ± 0.08 nm
Rg: 1.10 ± 0.03 nm
1.0 GHz, 0.7 V/nm
Clusters: 1471 (7.10%)
N-C Dist: 3.48 ± 0.10 nm
Rg: 1.04 ± 0.03 nm
2.5 GHz, 0.7 V/nm
Clusters: 2519 (0.88%)
N-C Dist: 3.4 ± 0.10 nm
Rg: 1.03 ± 0.03 nm
5.0 GHz, 0.7 V/nm
Clusters: 2832 (0.35%)
N-C Dist: 0.733± 0.23 nm
Rg: 0.59 ± 0.01 nm
(c)
0 GHz, 0.07 V/nm
Clusters: 429 (5.81%)
N-C Dist: 1.95 ± 0.13 nm
Rg:0.62 ± 0.02 nm
1.0 GHz, 0.07 V/nm
Clusters: 322 (18.22%)
N-C Dist: 0.45 ± 0.11 nm
Rg : 0.61 ± 0.01 nm
2.5 GHz, 0.07 V/nm
Clusters: 230 (17.79%)
N-C Dist: 0.50 ± 0.10nm
Rg: 0.60 ± 0.02 nm
5.0 GHz, 0.07 V/nm
Clusters: 333 (9.02%)
N-C Dist: 0.512 ± 0.10 nm
Rg: 0.589 ± 0.01 nm

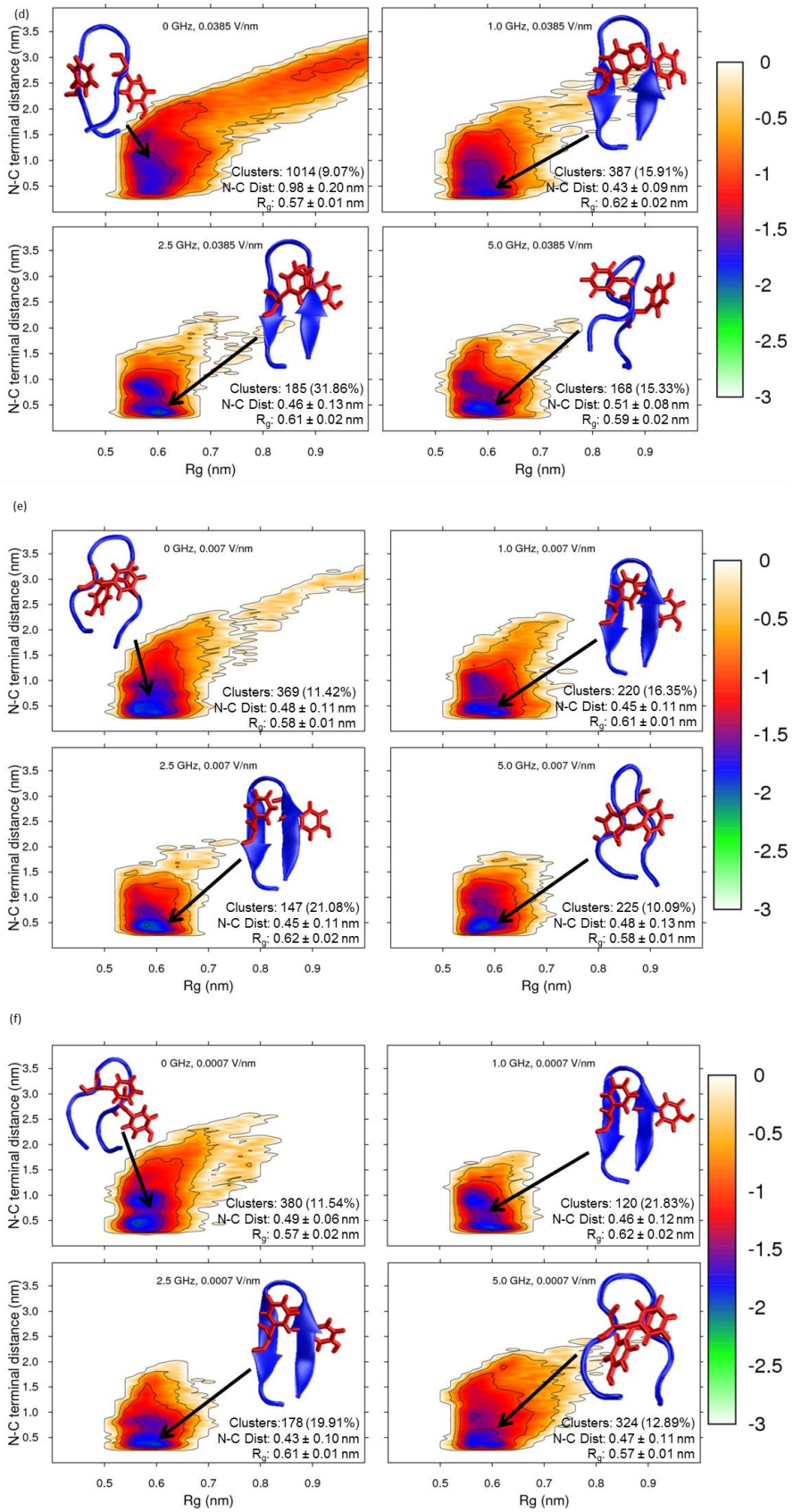

Figure 15: Free Energy Map (FEM) of the radius of gyration (Rg) vs N-C terminal distance determined for each ensemble trajectory of a) ambient; and static and oscillating (1.0-5.0 GHz) EM fields of b) 0.7 V/nmrms, c) 0.07 V/nmrms, d) 0.0385 V/nmrms, e) 0.007 V/nmrms, f) 0.0007 V/nmrms. The total number of clusters along with the percentage population of the most populated cluster identified and its structure are shown as insets. The average N-C distance and Rg of the structures belonging to the most populated cluster are also shown and identified on the FEM with an arrow on the FEM.

The free energy was calculated using $-k_BT \log(N)$, where $-k_B$ is Boltzmann's constant, T is temperature, and N_i is the total number of structures contained within a cluster *i* of the two properties measured on all structures within the ensemble trajectory for each field condition. Furthermore, the most visited region on the FEM was determined by calculating the average of each property from the structures contained within the most populated cluster of each EM field ensemble simulation, shown as insets in Figure 15.

The results from our recent static field simulations [83] showed that the high strength field (0.7 V/nm_{rms}) produces a distinct energy well or a "hot-spot", centred around ~3.5 nm N-C terminal distance separation and ~1.1 R_g, illustrating the peptides conformation is elongated. The unidirectional nature of the field along with the high strength, prevent the peptide from relaxing and adopting more compact native-like conformations. While the oscillatory nature of the fields of different frequencies and at high field strength provides an opportunity for the peptide to experience the condition of reduced or no external force, albeit for a short time. Figure 15 shows the gradual extension of the FEM highly populated region of elongated conformations towards the area of more compact, β-hairpin-like structures, as the field frequency is increased to 1 and 2.5 GHz. This suggests that the low to intermediate field frequencies provide sufficient time for the peptide to experience a change in conformation. In contrast, the 5 GHz simulations did not produce a recognisable "hot-spot" on the FEM, suggesting the peptide experiences continuous conformational changes, as the clustering analysis demonstrated. This result suggests that the field's high strength and frequency prevent the peptide from adopting specific conformation, in polar contrast to the results seen for the static or lower frequency simulations.

The static field simulations at intermediate field strengths (0.07-0.0385 V/nm_{rms}) exhibited more compact structures (N-C dist: 1.95 and 0.98 nm; Rg: 0.62 and 0.57 nm, respectively), however regions of elongated structures were also explored, as the FEM in Figure 15c,d shows. The introduction of frequency at these field strengths completely changed the conformational landscape explored by the peptide. The low (1.0 GHz) and the intermediate (2.5 GHz) frequencies specifically, confined the peptide to more compact β-hairpin conformations (0.0385 V/nm_{rms} N-C dist: 0.43 and 0.45 nm; Rg: 0.62 and 0.61 nm, respectively), while elongated structures were barely visited. Such kinetic-trapping could stimulate peptide self-assembly and promote the development of amyloid fibrils by apoC-II(60-70) peptide, as the β-hairpin arrangement was identified to be an intermediate state on-route for fibril formation [144]. The 5 GHz simulations, in contrast to the lower frequencies,

sampled structures with a more elongated conformation, demonstrated by the spreading of the FEM into higher N-C distance/Rg regions (N-C dist: 0.51 nm; Rg: 0.59 nm). The increased peptide dynamics due to the high field frequency can potentially prevent the formation of fibril-promoting states and in-turn inhibit or slow down the fibril-forming process.

The static low field strength (< 0.007 V/nm_{rms}) simulations produced mostly compact β-hairpin conformations (N-C dist: 0.48 and 0.49 nm; Rg: 0.58 and 0.57 nm, respectively), however the FEM showed also some exploration of more elongated structures, which is more evident in the 0.007 V/nm_{rms} simulations. The introduction of the oscillating fields completely abolished the exploration of these elongated states, and there is evident prevalence of more compact structures. The simulations at the three different frequencies sampled structures with similar conformational properties (0.0007 V/nm_{rms} N-C dist: 0.46, 0.43 and 0.47 nm; Rg: 0.62, 0.61 and 0.57 nm, for the 1, 2.5 and 5 GHz simulations, respectively). These results show that low strength fields of different (low, intermediate and high) frequencies have a negligible effect on the peptide conformation. Similarly, to the low strength static field simulations, the alternating field simulations also produced structures with fibril-forming conformations, as seen in Figure 15f.

Aromatic angles orientation

Hydrophobic interactions, specifically between aromatic side-chains, have an important role in the structure and function of proteins, as well as the formation and stabilisation of amyloid fibrils [78, 83]. In our previous studies we have shown that the two aromatic rings present in apoC-II(60-70) peptide, in particular, their orientation relative to the peptide "face" have a critical role in the peptide's mechanisms of aggregation [144]. Under fibril-inhibiting conditions, the aromatic rings are facing the same face of the peptide with relative angles < 90°, while under fibril-favouring conditions the relative angles between the aromatic residues are > 90°, which supports the formation of π-stack interactions with neighbouring peptides [76, 82, 144]. The EM forces can also affect the relative distribution of angles between the two aromatic rings, as demonstrated in our recent work [83]. Here to investigate the potential role of the field frequency on the peptide's aromatic side-chain characteristics (fibril-forming/inhibiting), the relative orientations of Tyr63 and Phe67 in apoC-II(60-70) was determined by calculating the average angle between the Cα-Cγ vector of Tyr63 and the Cα-

Cγ of Phe67. Figure 16 shows the population of structures (as percentage) with respect to the relative orientation (as angle) of the peptide's aromatic rings. A total of 40 bins were used over the range 0°–180°, with each data point corresponding to an angle interval of 4.5°.

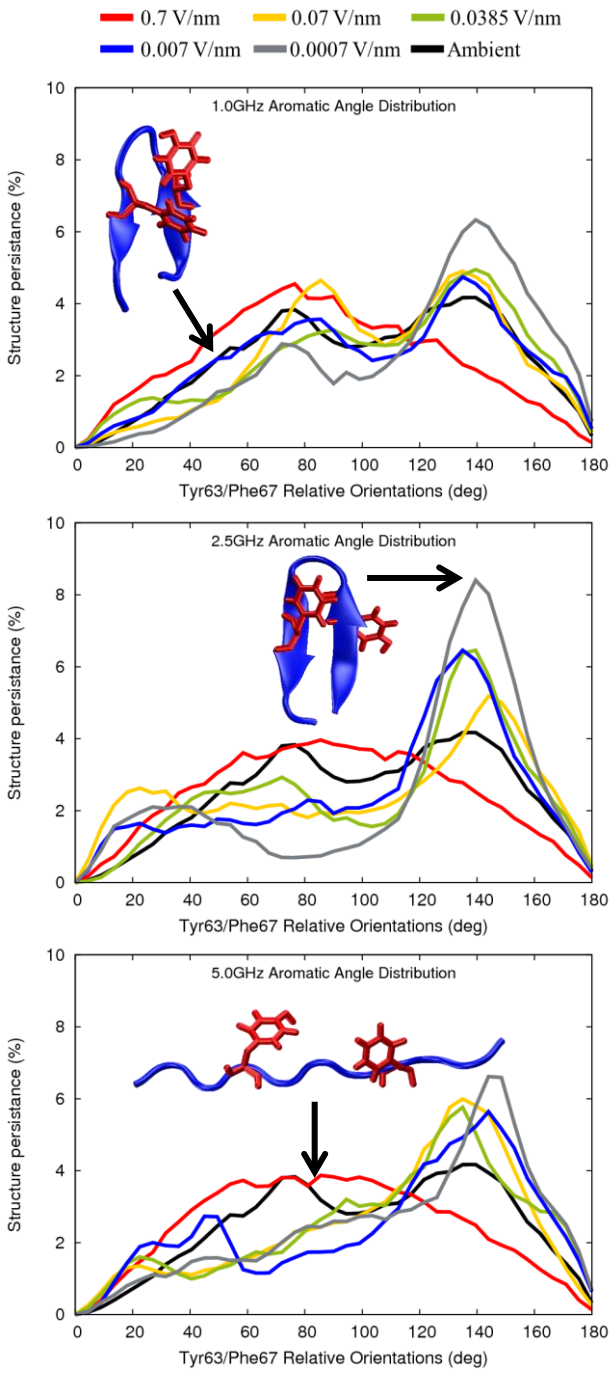

Figure 16: Histograms of the relative angle between Tyr63 and Phe67 (x-axis) over the concatenated trajectory of a) 1.0, b) 2.5 and c) 5.0 GHz simulations for each field strength. For comparison, the results from the ambient simulation is shown in black. Exemplar structures (secondary structure coloured in blue) and the relative aromatic side-chain arrangement (liquorice, red) a) fibril-inhibiting (0.007 V/nmrms), b) fibril-forming (0.0007 V/nmrms) and c) fibril-forming (0.7 V/nmrms) are shown as insets.

The results from the high strength field simulations exhibited a broad distribution of aromatic angles across all frequencies investigated, similar to those seen from the study on static fields [83]. The increased conformational dynamics due to the alternating fields prevented the peptide from adopting a stable (or preferred) aromatic arrangement. The 1 GHz oscillating EM fields of intermediate strength (0.07 and 0.0385 V/nm_{rms}) produced structures with aromatic residues present on the same face (85.5° and 90°, respectively) and opposite face (135° and 139.5°, respectively) of the peptide, identified by two distinct aromatic angle peaks in Figure 16a. The results are comparable to the static field simulations of the same field strengths where the peptide exhibited both fibril-favouring and fibril-inhibiting aromatic angle characteristics [83]. Interestingly, as the field frequency is increased to 2.5 and 5 GHz, there is a gradual shift for aromatic angle preference for the opposite face of the peptide (135-144°) at both field strengths. As seen from the FEMs in Figure 16, the low and intermediate frequencies have the ability to trap the peptide in specific conformations, and the aromatic angle results demonstrate that these conformations can have both fibril-forming or fibril-inhibiting characteristics. While the high frequency simulations produced slightly broader peaks compared to the 2.5 GHz fields due to the increased peptide dynamics, demonstrated earlier.

The low field strength (0.007-0.0007 V/nm_{rms}) simulations of all three frequencies produced structures with aromatic residues present on both faces of the peptide, in agreement with the static field and ambient results. This suggests the peptides exhibit fibril-favouring elements at low field strengths despite the modulation of the external force. Interestingly, the aromatic angle peaks for the 2.5 GHz low field strength simulations were also much narrower compared to the 1 and 5 GHz angle distributions at the low and intermediate field strengths, confirming the kinetic “trapping” ability of this microwave frequency.

Peptide dipole moment orientation

It is well known that applied fields have a direct effect on the molecules dipole moments. The applied field must be of specific strength to induce translational and/or rotational motion of the molecule in order to align itself along the applied field direction, as seen in our previous works [83] and others [90, 140]. This is highly dependent on the size and atomic charge distribution of the molecule itself. To determine the interrelation of the peptide dipole

moment and applied oscillating fields, the dipole autocorrelation function was calculated for each field strength/frequency condition and compared to the ambient and static field results (Figure 17). Our previous study showed that static field of high field strength (> 0.3 V/nm_{rms}) was sufficient to obtain complete alignment of the apoC-II(60-70) peptide dipole moment along the direction of the applied field [83]. There was an evident reduction in alignment correlation as the field strength was decreased down to 0.007 V/nm_{rms} field strength where there was no correlation between the field and the peptide dipole moment. Our simulations showed that field frequency has a strong effect on the peptide dipole association with the applied field. Highest correlation with the applied sinusoidal field was observed for the high field strength simulations (0.7 V/nm_{rms}) at all three frequencies. The 1 GHz simulations exhibited similar results to those of the static field, where the intermediate field strength also exhibited some alignment with the peptide dipole, albeit being significantly smaller compared to the high field strength simulation. In contrast, the 2.5 GHz simulations showed a barely noticeable correlation at intermediate field strengths, while the 5 GHz simulations showed no correlation at field strengths less than 0.07 V/nm_{rms}.

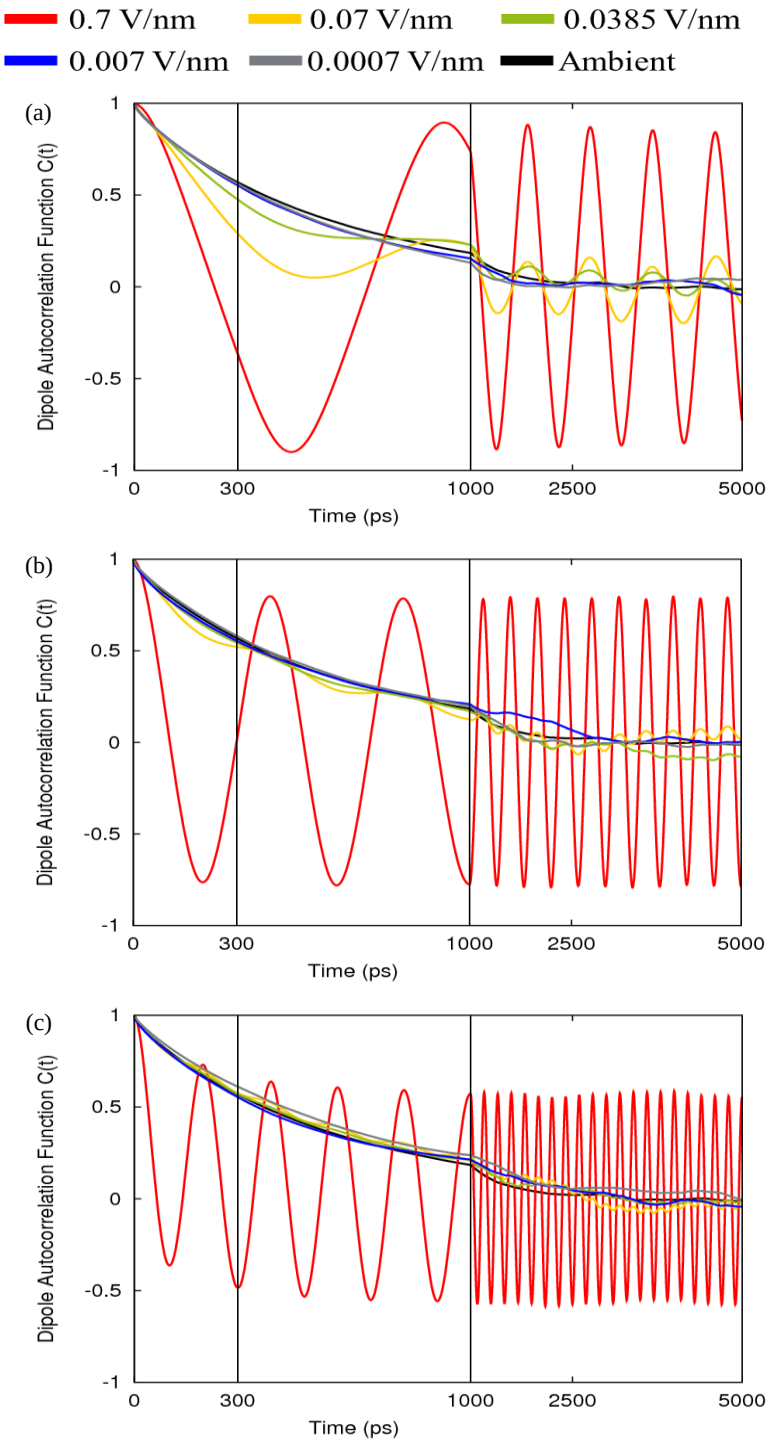

Figure 17: Peptide dipole autocorrelation function for each effective field strength at (a) 1 GHz, (b) 2.5 GHz and (c) 5.0 GHz frequency.

Peptide - water interactions

Water structuring and peptide-water interactions have an important role in the conformations peptides adopt, their dynamics, and most importantly, function. The specific peptide-solvent interactions were evaluated by radial distribution functions (RDF) over the equilibrium stage of each trajectory (Figure 18). The oscillating field simulations showed similar water structuring to that exhibited by the static field simulations [83], where three distinct hydration peaks were identified, the first two forming the first hydration shell (~0.185 and ~0.30 nm) indicating hydrogen bonding between the peptide and water, and the second hydration shell at ~0.45 nm. The most notable difference in the local density of water due to the applied field frequency can be seen at the high field strength simulations. Compared to the static field simulations [83], a small decrease in water packing can be observed with increasing field frequency, caused by the continuous change in conformation and the formation of compact β-hairpin-like structures (Figure 18c,d). At intermediate (0.07-0.0385 V/nm_{rms}) and low field strengths (0.007-0.0007 V/nm_{rms}) the presence of the oscillating field does not have any effect on the water packing, regardless of the field frequency applied. This is due to the peptide being trapped in β-hairpin and β-hairpin-like conformations that are less solvated than the conformations explored at high field strengths, as is seen in our previous static field simulations.

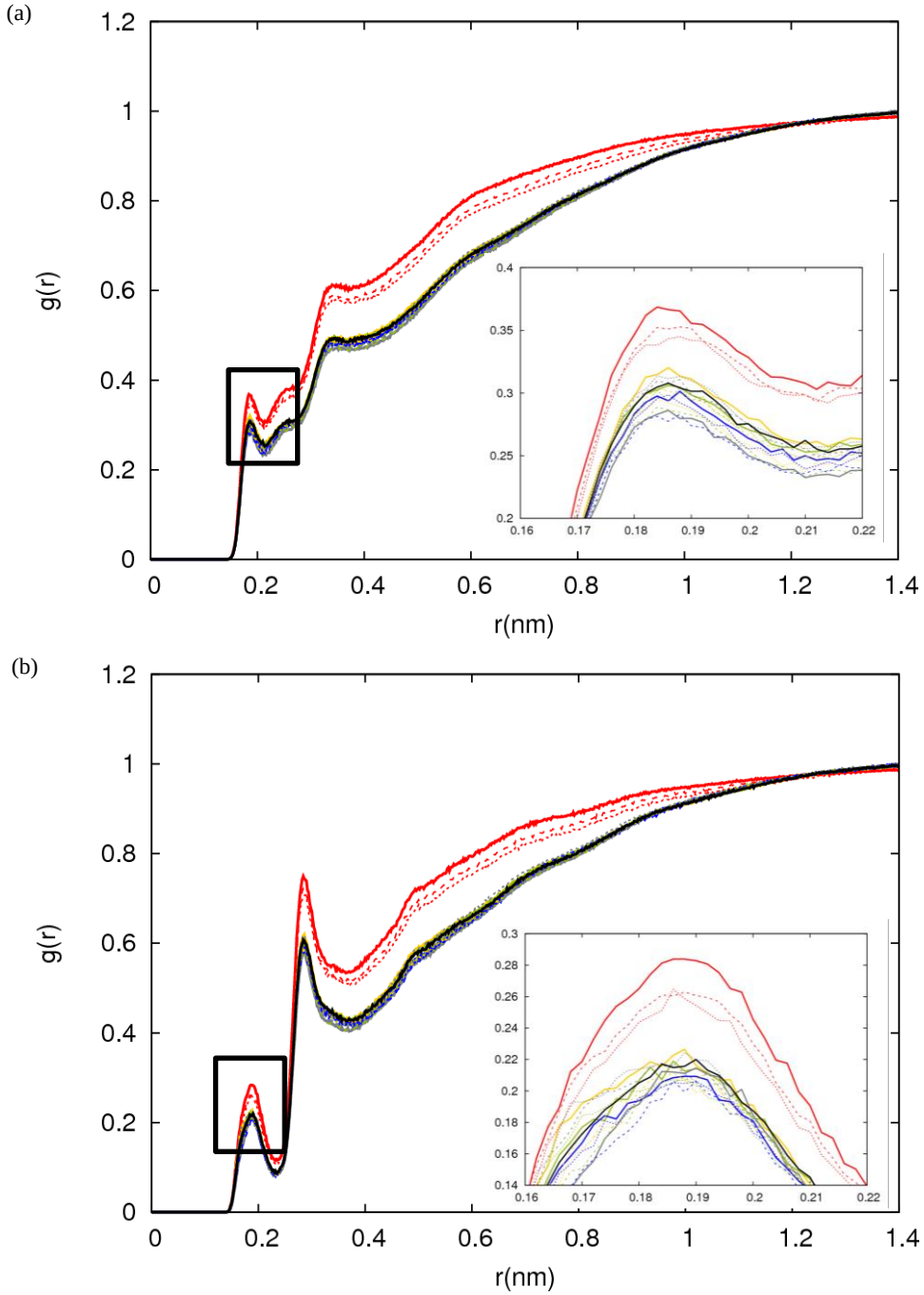

Figure 18: Peptide-water interactions represented by radial distribution functions of (a) peptide (NHO)-water (H) and (b) peptide (NHO)-water (O). The RDFs for 1.0 GHz are shown as solid lines, 2.5 GHz as dashes, and 5.0 GHz as dots. Line colour to represent field strength: 0.7 V/nm_{rms} (red), 0.07 V/nm_{rms} (yellow), 0.0385 V/nm_{rms} (green), 0.007 V/nm_{rms} (blue), 0.0007 V/nm_{rms} (grey), ambient (black).

Conclusion

All-atom non-equilibrium molecular dynamics simulations were performed to investigate the amyloidogenic apoC-II(60-70) peptide response to oscillating EM fields of different frequency and strength. Our results showed that the applied oscillating fields induced unique peptide conformations with different fibril-forming propensities that are dependent on the field characteristics. The exposure of apoC-II(60-70) to alternating high strength fields (0.7 V/nm_{rms}) of 1.0 to 5 GHz frequency promoted a significant increase in the peptide dynamics, compared to the static field simulations [83]. This suggested there is an immediate conformational response to the applied field direction and strength. Specifically, the 1 and 2.5 GHz simulations exhibited some conformation preference, as indicated by frequently explored regions or free-energy map "hot-spots" with similar N-C terminal spacing and radius of gyration, the 5 GHz simulations sampled wider-conformational space due to the faster oscillations. In contrast, the intermediate field strength (0.07-0.0385 V/nm_{rms}) simulation of 1.0 and 2.5 GHz frequency were able to restrain or kinetically trap the peptide in specific conformations, demonstrated by the higher conformational stability and lower number of clusters explored by these trajectories compared to the static field simulation at the same effective strength. Although, the structures sampled from the different frequency simulations were very similar, i.e. β-hairpin-like, they exhibited different fibril-forming characteristics. The 1.0 GHz simulations explored structures with aromatic rings on the same as well as both sides of the peptide, indicating structures with fibril-forming and/or fibril-inhibiting propensities, while the 2.5 GHz simulations showed preference for the fibril-forming arrangement of the aromatic rings. The results suggest that the "trapping" ability of the 1.0 and especially 2.5 GHz fields of intermediate strength can have a binary effect on fibril formation of apoC-II(60-70) peptide. In contrast to the lower frequency results, the 5 GHz simulations showed increased peptide dynamics, more extended structures and aromatic side-chain arrangements on the opposite face of the peptide, similar to those seen in the ambient simulations. This suggests the field oscillations or change in field direction is so frequent that it prevents the peptide from being restrained in a particular conformation or aromatic arrangement. Interestingly, the low strength fields (0.007-0.0007 V/nm_{rms}) at all frequencies exhibited amyloid-prone hairpin conformations similar to those seen in the ambient and static field simulations of the same effective strength. This result is in line with peptide dipole-field interrelation analysis, which showed complete loss of peptide dipole-field correlation at field strengths lower than 0.04 V/nm. The highest correlations were

evident for high strength (0.7 V/nm_{rms}) and the low frequency (1.0 GHz) simulations. The peptide dipole-field correlation dissipated significantly as the frequency was increased to 2.5 and 5 GHz. While the water structuring in the close proximity of the peptide was similar to those observed under static fields, i.e. formation of 2 hydration shells; higher water density (increased solvation) was observed high strength/low frequency simulations due to the continuous transitions between elongated and compact states, compared to the lower frequency simulation which explored more compact (less solvated) states. Overall, our results showed that peptides exhibit a strong conformational dependence on the applied field strength and frequency. Specific field parameter combinations can be designed to produce peptides with structural characteristics that can prevent or inhibit their self-assembly, which can be used as an alternative method for the prevention or treatment of amyloid fibrils. At the same time, field parameters can be chosen to promote the growth of well-ordered peptide assemblies for the development of biocompatible nanomaterials.

Chapter 5
Conclusions

EM fields have become a ubiquitous part of modern day life and the interactions between these fields and human biology needs to be researched to ensure that there aren't any deleterious effects being experienced by humanity. Current research is divided on the potential health effects, beneficial or detrimental of EM field exposure, with some researchers claiming an increase in cancer and glioma occurrence, while other researchers are investigating its uses in wound healing and treatment for/prevention against Alzheimer's plaques. In this thesis, the effects of EM field on the apoC-II(60-70) peptide monomer derivative was modelled under EM field at various strengths and frequencies to observe the atomistic effects of the various fields on the peptide response in an aqueous environment.

The static field simulation studies presented in Chapter 3 showed that the field strength has a significant effect on the peptide conformation and dynamics. High field strengths caused the peptide to elongate along the external field and lose its inherent β-hairpin structure, due to the dipole alignment effects of the electric field component. In the "intermediate" field strength range the simulations showed intriguing behaviour by the apoC-II(60-70) peptide, where some differences between the EM- and electric field-induced structures became more apparent. The peptide was significantly more dynamic in this field range, and in the EM field simulations, adopted conformational characteristics typical for its fibril-inhibiting behaviour, well-separated N- and C-termini are prominent and aromatic-ring locations having a preference for the same face of the peptide. Differences could also be seen between EM and electric field effects on the peptide free-energy landscape, with EM field being able to trap the peptide in twisted (non-β-hairpin like) conformations and limit conformational space, in contrast to the simulations where the peptide was found to be more dynamic and adopted predominantly β-hairpin-like structures. The low-strength simulations produced stable β-hairpin peptide conformations similar to ambient conditions, as the aromatic Tyr63/Phe67 pair showed preference for the opposite faces of the peptide, suggesting a fibril-forming peptide capacity at such conditions.

Despite the extensive simulation times and relatively thorough sampling, the question remains as to whether the nuances observed in the peptide's conformational preferences between electric and EM field was in fact caused by the additional magnetic force, or by the finite nature of the simulations. Analysis of the peptide and water dipoles was able to show that field strength of at least 0.007 V/nm was necessary to observe any field effects. Most importantly, the results suggests that EM field could be considered for designing alternative treatments of amyloid diseases due to its inhibiting effect on the amyloidogenic peptide conformations for the intermediate strength, whilst the very high- and low-field strengths stabilising amyloid favourable peptide conformations could be employed for engineering well-ordered peptide assemblies for other applications.

Chapter 4 results showed that the application of oscillating fields induced unique peptide conformations with different fibril-forming propensities dependent on the field characteristics. The exposure of apoC-II(60-70) to alternating high strength fields (0.7 V/nm_{rms}) of 1.0 to 5 GHz frequency promoted a significant increase in the peptide dynamics, when compared to the static field simulations in Chapter 3, suggesting that there is an immediate conformational response to the applied field direction and strength. Specifically, the 1 and 2.5 GHz simulations exhibited some conformation preference, indicated by frequent free-energy map "hot-spots" with similar N-C terminal spacing and radius of gyration. The 5 GHz simulations sampled a wider-conformational space due to the faster oscillations.

The intermediate field strength simulation of 1.0 and 2.5 GHz frequency were able to kinetically trap the peptide in specific conformations, demonstrated by the higher conformational stability and lower number of clusters explored by these trajectories compared to the previous static field simulation at the same effective strength. Although, the structures sampled from the different frequency simulations were very similar (β-hairpin-like) they exhibited different fibril-forming characteristics, with 1.0 GHz simulations exploring structures with aromatic rings on the same and opposing sides of the peptide, indicating structures with fibril-forming and/or fibril-inhibiting propensities, while the 2.5 GHz simulations showed preference for the fibril-forming arrangement of the aromatic rings. The results suggest that the "trapping" ability of the 1.0 and especially 2.5 GHz fields of intermediate strength can have a binary effect on fibril formation of apoC-II(60-70) peptide. In contrast, the 5 GHz simulations showed increased peptide dynamics, more extended structures and aromatic side-chain arrangements on the opposite face of the peptide, similar to those seen in the ambient simulations. This suggests the field oscillations or change in field

direction is so frequent that it prevents the peptide from being restrained in a particular conformation or aromatic arrangement.

Interestingly, the low strength fields (0.007-0.0007 V/nm_{rms}) at all frequencies exhibited amyloid-prone hairpin conformations similar to those seen in the ambient and static field simulations of the same effective strength. This result is in line with peptide dipole-field interrelation analysis, which showed complete loss of peptide dipole-field correlation at field strengths lower than 0.04 V/nm. The highest correlations were evident for high strength (0.7 V/nm_{rms}) and the low frequency (1.0 GHz) simulations. The peptide dipole-field correlation dissipated significantly as the frequency was increased to 2.5 and 5 GHz. While the water structuring in the close proximity of the peptide was similar to those observed under static fields, i.e. formation of 2 hydration shells; higher water density (increased solvation) was observed high strength/low frequency simulations due to the continuous transitions between elongated and compact states, compared to the lower frequency simulation which explored more compact (less solvated) states.

Overall, the results from chapter 4 showed that peptides exhibit a strong conformational dependence on the applied field strength and frequency. With this knowledge it could become possible for future researchers to investigate the possibility of being able to craft protein assemblies for medicinal purposes, such as biocompatible nanomaterials, or to make proteins designed to inhibit the formation of amyloid fibrils. Another use for the tuning of EM fields could result in finding parameters that can be used to treat amyloid diseases through disruption of plaques with non-invasive methods.

Future investigation of protein fibrils and amyloidogenic proteins will involve the combined efforts of theoretical and experimental collaborators. Further study of the effects of proteins may be investigating fibril formation rates through sedimentation analysis and then these structures being exposed to EM fields and characterised using real time autofluorescence and Circular Dichroism spectroscopy. These techniques will provide quantitative information on the shear rates and solution conformation of peptide/aggregates under the influence of different fields and intensities, which can be compared to the modelling results presented here.

The aims of this thesis was to study and elucidate the effects of EM fields on the apoC-II(60-70) peptide derivative to be able to provide a stepping stone of fundamental research into

furthering theoretical and experimental studies of EM fields so that new (smart) technology and medical uses of EM fields can be developed with greater understanding.

References

1. Apollonio, F., et al., *Feasibility for microwaves energy to affect biological systems via nonthermal mechanisms: A systematic approach.* IEEE Transactions on Microwave Theory and Techniques, 2013. **61**(5): p. 2031-2045.
2. Budi, A., et al., *Electric field effects on insulin chain-B conformation.* Journal of Physical Chemistry B, 2005. **109**(47): p. 22641-22648.
3. Budi, A., et al., *Comparative study of insulin chain-B in isolated and monomeric environments under external stress.* Journal of Physical Chemistry B, 2008. **112**(26): p. 7916-7924.
4. Caraglia, M., et al., *Electromagnetic fields at mobile phone frequency induce apoptosis and inactivation of the multi-chaperone complex in human epidermoid cancer cells.* Journal of Cellular Physiology, 2005. **204**(2): p. 539-548.
5. Challis, L.J., *Mechanisms for interaction between RF fields and biological tissue.* Bioelectromagnetics, 2005. **Suppl 7**(S7): p. S98-S106.
6. de Pomerai, D.I., et al., *Microwave radiation can alter protein conformation without bulk heating.* Febs Letters, 2003. **543**(1-3): p. 93-97.
7. English, N.J. and C.J. Waldron, *Perspectives on external electric fields in molecular simulation: progress, prospects and challenges.* Physical Chemistry Chemical Physics, 2015. **17**(19): p. 12407-12440.
8. Gaestel, M., *Biological monitoring of non-thermal effects of mobile phone radiation: recent approaches and challenges.* Biological Reviews, 2010. **85**(3): p. 489-500.
9. Humans, I.W.G.o.t.E.o.C.R.t., *Non-ionizing radiation, Part 2: Radiofrequency electromagnetic fields.* Iarc Monographs on the Evaluation of Carcinogenic Risks to Humans, 2013. **102**(PT 2): p. 1-460.
10. Loughran, S.P., et al., *Bioelectromagnetics Research within an Australian Context: The Australian Centre for Electromagnetic Bioeffects Research (ACEBR).* International Journal of Environmental Research and Public Health, 2016. **13**(10): p. 967.
11. Adey, W.R., *Biological effects of electromagnetic fields.* Journal of Cellular Biochemistry, 1993. **51**(4): p. 410-416.
12. Porcelli, M., et al., *Non-thermal effects of microwaves on proteins: Thermophilic enzymes as model system.* Febs Letters, 1997. **402**(2-3): p. 102-106.
13. Mancinelli, F., et al., *Non-thermal effects of electromagnetic fields at mobile phone frequency on the refolding of an intracellular protein: Myoglobin.* Journal of Cellular Biochemistry, 2004. **93**(1): p. 188-196.
14. English, N.J. and D.A. Mooney, *Denaturation of hen egg white lysozyme in electromagnetic fields: a molecular dynamics study.* Journal of Chemical Physics, 2007. **126**(9): p. 091105.
15. English, N.J., G.Y. Solomentsev, and P. O'Brien, *Nonequilibrium molecular dynamics study of electric and low-frequency microwave fields on hen egg white lysozyme.* Journal of Chemical Physics, 2009. **131**(3): p. 035106.
16. Laurence, J.A., et al., *Biological effects of electromagnetic fields--mechanisms for the effects of pulsed microwave radiation on protein conformation.* Journal of Theoretical Biology, 2000. **206**(2): p. 291-298.
17. Xie, Y., et al., *Modulating protein behaviors on responsive surface by external electric fields: A molecular dynamics study.* Applied Surface Science, 2015. **326**: p. 55-65.
18. Zhao, W., et al., *Review: pulsed electric fields processing of protein-based foods.* Food and Bioprocess Technology, 2014. **7**(1): p. 114-125.
19. Repacholi, M.H., *Health risks from the use of mobile phones.* Toxicology Letters, 2001. **120**(1-3): p. 323-331.

20. Bohr, H. and J. Bohr, *Microwave-enhanced folding and denaturation of globular proteins.* Physical Review E, 2000. **61**(4): p. 4310-4314.
21. Weissenborn, R., et al., *Non-thermal microwave effects on protein dynamics? An X-ray diffraction study on tetragonal lysozyme crystals.* Acta Crystallogr D Biol Crystallogr, 2005. **61**(Pt 2): p. 163-72.
22. Rejasse, B., et al., *Influence of microwave radiation on free Candida antarctica lipase B activity and stability.* Org Biomol Chem, 2006. **4**(19): p. 3703-7.
23. Maziarz, A., et al., *How electromagnetic fields can influence adult stem cells: positive and negative impacts.* Stem Cell Research & Therapy, 2016. **7**(1): p. 54.
24. Redmayne, M. and O. Johansson, *Could myelin damage from radiofrequency electromagnetic field exposure help explain the functional impairment electrohypersensitivity? A review of the evidence.* Journal of Toxicology and Environmental Health, Part B: Critical Reviews, 2014. **17**(5): p. 247-258.
25. Kim, K.-H., E. Kabir, and S.A. Jahan, *The use of cell phone and insight into its potential human health impacts.* Environmental Monitoring and Assessment, 2016. **188**(4): p. 221.
26. Saygin, M., et al., *Impact of 2.45 GHz microwave radiation on the testicular inflammatory pathway biomarkers in young rats: The role of gallic acid.* Environmental Toxicology, 2015. **31**(12): p. 1771-1784.
27. Liu, X., et al., *Effects of extremely low frequency electromagnetic field on the health of workers in automotive industry.* Electromagnetic Biology and Medicine, 2013. **32**(4): p. 551-559.
28. Phillips, J.L., N.P. Singh, and H. Lai, *Electromagnetic fields and DNA damage.* Pathophysiology, 2009. **16**(2-3): p. 79-88.
29. Vadala, M., et al., *Mechanisms and therapeutic effectiveness of pulsed electromagnetic field therapy in oncology.* Cancer Medicine, 2016. **5**(11): p. 3128-3139.
30. Arendash, G.W., *Transcranial electromagnetic treatment against Alzheimer's disease: why it has the potential to trump Alzheimer's disease drug development.* Journal of Alzheimer's Disease, 2012. **32**(2): p. 243-266.
31. Arendash, G.W., *Review of the Evidence that Transcranial Electromagnetic Treatment will be a Safe and Effective Therapeutic Against Alzheimer's Disease.* Journal of Alzheimer's Disease, 2016. **53**(3): p. 753-771.
32. Arendash, G.W., C. Cao, and J. Tan, *Prevention and treatment of brain diseases and disorders related to abnormal protein aggregation through electromagnetic field treatment*. 2016, University of South Florida (Tampa, FL, US).
33. Saliev, T., et al., *Therapeutic potential of electromagnetic fields for tissue engineering and wound healing.* Cell Proliferation, 2014. **47**(6): p. 485-493.
34. Ashrafi, M., et al., *The efficacy of electrical stimulation in experimentally induced cutaneous wounds in animals.* Veterinary Dermatology, 2016. **27**(4): p. 235-e57.
35. Daish, C., et al., *The Application of Pulsed Electromagnetic Fields (PEMFs) for Bone Fracture Repair: Past and Perspective Findings.* Ann Biomed Eng, 2018. **46**(4): p. 525-542.
36. Arendash, G.W., et al., *Electromagnetic field treatment protects against and reverses cognitive impairment in Alzheimer's disease mice.* Journal of Alzheimer's Disease, 2010. **19**(1): p. 191-210.
37. Arendash, G.W., et al., *Electromagnetic treatment to old Alzheimer's mice reverses beta-amyloid deposition, modifies cerebral blood flow, and provides selected cognitive benefit.* PLoS One, 2012. **7**(4): p. e35751.
38. Arendash, G.W., C. Cao, and J. Tan, *Prevention and treatment of alzheimer's disease through electromagnetic field exposure*. 2012, Google Patents.
39. askIITians, *a-Helix and beta -sheet structure of protein*, 2014730-121956716-1038-mga2-03-25.jpg, Editor. 2018, askiitians: Peptide and Proteins.
40. Ramachandran, G.N. and V. Sasisekharan, *Conformation of Polypeptides and Proteins*, in *Advances in Protein Chemistry Volume 23*. 1968. p. 283-437.
41. Chothia, C., *The nature of the accessible and buried surfaces in proteins.* Journal of Molecular Biology, 1976. **105**(1): p. 1-14.

42. Astbury, W.T., S. Dickinson, and K. Bailey, *The X-ray interpretation of denaturation and the structure of the seed globulins.* Biochem J, 1935. **29**(10): p. 2351-2360 1.
43. Cohen, A.S. and E. Calkins, *Electron microscopic observations on a fibrous component in amyloid of diverse origins.* Nature, 1959. **183**(4669): p. 1202-3.
44. Fruhling, L., J. Kempf, and A. Porte, *[Structure and formation of the amyloid substance in experimental amyloidosis in the mouse. Electron microscopic study].* C R Hebd Seances Acad Sci, 1960. **250**: p. 1385-6.
45. Caesar, R., *Die Feinstruktur Von Milz Und Leber Bei Experimenteller Amyloidose.* Zeitschrift Fur Zellforschung Und Mikroskopische Anatomie, 1960. **52**(5): p. 653-673.
46. Battaglia, S., *[Electronoptic studies on liver amyloid in mice].* Beitr Pathol Anat, 1962. **126**: p. 300-20.
47. Cohen, A.S., et al., *A study of the fine structure of the amyloid associated with familial Mediterranean fever.* Am J Pathol, 1962. **41**: p. 567-78.
48. Heefner, W.A. and G.D. Sorenson, *Experimental amyloidosis. I. Light and electron microscopic observation of spleen and lymph nodes.* Lab Invest, 1962. **11**: p. 585-93.
49. *Research: Amyloid Protein*. Griffin Group: Griffin Group: Spinning All The Hits. p. Background image of triplet TTR(105-115) fibril taken using TEM (Left). TTR(105-115) triplet fibril fitted into cryo-EM reconstruction (Center and Right).
50. Ryan, T.M., et al., *The Role of Lipid in Misfolding and Amyloid Fibril Formation by Apolipoprotein C-II*, in *Advances in Experimental Medicine and Biology*. 2015. p. 157-174.
51. Griffin, M.D.W., et al., *Phospholipid interaction induces molecular-level polymorphism in apolipoprotein C-II amyloid fibrils via alternative assembly pathways.* Journal of Molecular Biology, 2008. **375**(1): p. 240-256.
52. Griffin, M.D.W., et al., *A cyclic peptide inhibitor of apoC-II peptide fibril formation: Mechanistic insight from NMR and molecular dynamics analysis.* Journal of Molecular Biology, 2012. **416**(5): p. 642-655.
53. Crescenzi, O., et al., *Solution structure of the Alzheimer amyloid β-peptide (1-42) in an apolar microenvironment.* European Journal of Biochemistry, 2002. **269**(22): p. 5642-5648.
54. Todorova, N., et al., *Intra- and Intersubunit Ion-Pair Interactions Determine the Ability of Apolipoprotein C-II Mutants To Form Hybrid Amyloid Fibrils.* Biochemistry, 2017. **56**(12): p. 1757-1767.
55. Mao, Y., et al., *Solution Conditions Affect the Ability of the K30D Mutation To Prevent Amyloid Fibril Formation by Apolipoprotein C-II: Insights from Experiments and Theoretical Simulations.* Biochemistry, 2016. **55**(27): p. 3815-3824.
56. Legge, F.S., et al., *Molecular dynamics simulations of a fibrillogenic peptide derived from apolipoprotein C-II.* Biophysical Chemistry, 2007. **130**(3): p. 102-113.
57. Todorova, N., *Molecular modelling of peptide folding, misfolding and aggregation phenomena*, in *School of Applied Sciences*. 2009, RMIT University: Melbourne.
58. Hung, A., et al., *Lipids enhance apolipoprotein C-II-derived amyloidogenic peptide oligomerization but inhibit fibril formation.* Journal of Physical Chemistry B, 2009. **113**(28): p. 9447-9453.
59. Hung, A., N. Todorova, and I. Yarovsky, *Computer simulation studies of abnormal protein aggregation*, in *Proceedings of the 2nd WSEAS International Conference on Biomedical Electronics and Biomedical Informatics*, C.A. Long, et al., Editors. 2009, WSEAS Press: Moscow, Russia. p. 41-46.
60. Todorova, N., A. Hung, and I. Yarovsky, *Application of computational modelling to protein folding and aggregation studies*, in *Proceedings of the 10th WSEAS International Conference on Mathematics and Computers in Biology and Chemistry*, N.E. Mastorakis, et al., Editors. 2009, WSEAS Press: Prague, Czech Republic. p. 130-135.
61. Musliner, T.A., P.N. Herbert, and E.C. Church, *Activation of lipoprotein lipase by native and acylated peptides of apolipoprotein C-II.* Biochimica et Biophysica Acta, 1979. **573**(3): p. 501-509.
62. Stewart, C.R., et al., *Serum amyloid P colocalizes with apolipoproteins in human atheroma: functional implications.* Journal of Lipid Research, 2007. **48**(10): p. 2162–2171.

63. Jong, M.C., M.H. Hofker, and L.M. Havekes, *Role of ApoCs in Lipoprotein Metabolism Functional Differences Between ApoC1, ApoC2, and ApoC3.* Arteriosclerosis, Thrombosis, and Vascular Biology, 1999. **19**(3): p. 472-484.
64. Medeiros, L.A., et al., *Fibrillar amyloid protein present in atheroma activates CD36 signal transduction.* Journal of Biological Chemistry, 2004. **279**(11): p. 10643–10648.
65. Segrest, J.P., et al., *The amphipathic helix in the exchangeable apolipoproteins: a review of secondary structure and function.* Journal of Lipid Research, 1992. **33**(2): p. 141-166.
66. MacRaild, C.A., G.J. Howlett, and P.R. Gooley, *The structure and interactions of human apolipoprotein C-II in dodecyl phosphocholine.* Biochemistry, 2004. **43**(25): p. 8084-8093.
67. Zdunek, J., et al., *Global structure and dynamics of human apolipoprotein CII in complex with micelles: evidence for increased mobility of the helix involved in the activation of lipoprotein lipase.* Biochemistry, 2003. **42**(7): p. 1872-1889.
68. Hatters, D.M., et al., *Human apolipoprotein C-II forms twisted amyloid ribbons and closed loops.* Biochemistry, 2000. **39**(28): p. 8276-8283.
69. Binger, K.J., et al., *Apolipoprotein C-II amyloid fibrils assemble via a reversible pathway that includes fibril breaking and rejoining.* Journal of Molecular Biology, 2008. **376**(4): p. 1116–1129.
70. Hatters, D.M. and G.J. Howlett, *The structural basis for amyloid formation by plasma apolipoproteins: a review.* European Biophysics Journal, 2002. **31**(1): p. 2-8.
71. Hatters, D.M., A.P. Minton, and G.J. Howlett, *Macromolecular crowding accelerates amyloid formation by human apolipoprotein C-II.* Journal of Biological Chemistry, 2002. **277**(10): p. 7824-7830.
72. Hatters, D.M., L.J. Lawrence, and G.J. Howlett, *Sub-micellar phospholipid accelerates amyloid formation by apolipoprotein C-II.* FEBS Letters, 2001. **494**(3): p. 220-224.
73. Binger, K.J., M.D.W. Griffin, and G.J. Howlett, *Methionine Oxidation Inhibits Assembly and Promotes Disassembly of Apolipoprotein C-II Amyloid Fibrils.* Biochemistry, 2008. **47**(38): p. 10208-10217.
74. Wilson, L.M., et al., *A structural core within apolipoprotein C-II amyloid fibrils identified using hydrogen exchange and proteolysis.* Journal of Molecular Biology, 2007. **366**(5): p. 1639-1651.
75. Howlett, G.J. and K.J. Moore, *Untangling the role of amyloid in atherosclerosis.* Current Opinion in Lipidology, 2006. **17**(5): p. 541–547.
76. Todorova, N., A. Hung, and I. Yarovsky, *Lipid Concentration Effects on the Amyloidogenic apoC-II60−70 Peptide: A Computational Study.* The Journal of Physical Chemistry B, 2010. **114**(23): p. 7974-7982.
77. Todorova, N. and I. Yarovsky, *Molecular modelling of peptide folding, misfolding and aggregation phenomena.* Procedia Computer Science, 2010. **1**(1): p. 1185-1193.
78. Todorova, N., et al., *Effects of mutation on the amyloidogenic propensity of apolipoprotein C-II(60-70) peptide.* Phys Chem Chem Phys, 2010. **12**(44): p. 14762-74.
79. Makarucha, A.J., N. Todorova, and I. Yarovsky, *Nanomaterials in biological environment: A review of computer modelling studies.* European Biophysics Journal, 2011. **40**(2): p. 103-115.
80. Teoh, C.L., et al., *A structural model for apolipoprotein C-II amyloid fibrils: Experimental characterization and molecular dynamics simulations.* Journal of Molecular Biology, 2011. **405**(5): p. 1246-1266.
81. Todorova, N. and I. Yarovsky, *Molecular modelling of peptide folding, misfolding and aggregation phenomena*, in *Procedia Computer Science*. 2012. p. 1185-1193.
82. Todorova, N., et al., *"Janus" cyclic peptides: a new approach to amyloid fibril inhibition?* PLOS One, 2013. **8**(2): p. e57437.
83. Todorova, N., et al., *Electromagnetic-field effects on structure and dynamics of amyloidogenic peptides.* Journal of Chemical Physics, 2016. **144**(8): p. 8.
84. Hung, A., et al., *Effects of oxidation, pH and lipids on amyloidogenic peptide structure: implications for fibril formation?* European Biophysics Journal, 2008. **38**(1): p. 99-110.
85. Todorova, N., et al., *Dimensionality of Carbon Nanomaterials Determines the Binding and Dynamics of Amyloidogenic Peptides: Multiscale Theoretical Simulations.* PLoS computational biology, 2013. **9**(12): p. e1003360.

86. Tekieh, T., P. Sasanpour, and H. RafiiTabar, *Effects of Electromagnetic Field Exposure on Conduction and Concentration of Voltage Gated Calcium Channels: A Brownian Dynamics Study*. Brain Reserach, 2016. **1646**: p. 560-569.
87. Toschi, F., et al., *Effects of electric field stress on a beta-amyloid peptide.* Journal of Physical Chemistry B, 2009. **113**(1): p. 369-76.
88. Marracino, P., et al., *Effect of High Exogenous Electric Pulses on Protein Conformation: Myoglobin as a Case Study.* Journal of Physical Chemistry B, 2013. **117**(8): p. 2273-2279.
89. English, N.J. and J.M.D. MacElroy, *Hydrogen bonding and molecular mobility in liquid water in external electromagnetic fields.* Journal of Chemical Physics, 2003. **119**(22): p. 11806-11813.
90. English, N.J. and J.M.D. MacElroy, *Molecular dynamics simulations of microwave heating of water.* Journal of Chemical Physics, 2003. **118**(4): p. 1589-1592.
91. English, N.J., *Molecular dynamics simulations of microwave effects on water using different long-range electrostatics methodologies.* Molecular Physics, 2006. **104**(2): p. 243-253.
92. Solomentsev, G.Y., N.J. English, and D.A. Mooney, *Hydrogen bond perturbation in hen egg white lysozyme by external electromagnetic fields: a nonequilibrium molecular dynamics study.* Journal of Chemical Physics, 2010. **133**(23): p. 235102.
93. Garate, J.A., N.J. English, and J.M. MacElroy, *Human aquaporin 4 gating dynamics in dc and ac electric fields: a molecular dynamics study.* Journal of Chemical Physics, 2011. **134**(5): p. 055110.
94. Reale, R., et al., *Human aquaporin 4 gating dynamics under and after nanosecond-scale static and alternating electric-field impulses: A molecular dynamics study of field effects and relaxation.* J Chem Phys, 2013. **139**(20): p. 205101.
95. English, N.J. and J.-A. Garate, *Near-microsecond human aquaporin 4 gating dynamics in static and alternating external electric fields: Non-equilibrium molecular dynamics.* Journal of Chemical Physics, 2016. **145**(8): p. 085102.
96. Budi, A., et al., *Effect of frequency on insulin response to electric field stress.* Journal of Physical Chemistry B, 2007. **111**(20): p. 5748-5756.
97. Alder, B.J. and T. Wainwright, *Studies in molecular dynamics. I. General method.* The Journal of Chemical Physics, 1959. **31**(2): p. 459-466.
98. Alder, B. and T. Wainwright, *Phase transition for a hard sphere system.* The Journal of Chemical Physics, 1957. **27**(5): p. 1208-1209.
99. Karplus, M. and J.A. McCammon, *Molecular dynamics simulations of biomolecules.* Nature Structural & Molecular Biology, 2002. **9**(9): p. 646-652.
100. Verlet, L., *Computer Experiments on Classical Fluids .I. Thermodynamical Properties of Lennard-Jones Molecules.* Physical Review, 1967. **159**(1): p. 98-+.
101. Hockney, R.W., S.P. Goel, and J.W. Eastwood, *Quiet high-resolution computer models of a plasma*. Journal of Computational Physics, 1974. **14**(2): p. 148-158.
102. Swope, W.C., et al., *A computer simulation method for the calculation of equilibrium constants for the formation of physical clusters of molecules: Application to small water clusters.* The Journal of Chemical Physics, 1982. **76**(1): p. 637-649.
103. Beeman, D., *Some multistep methods for use in molecular dynamics calculations.* Journal of Computational Physics, 1976. **20**(2): p. 130-139.
104. Bekker, H., et al., *An Efficient, Box Shape Independent Non-Bonded Force and Virial Algorithm for Molecular Dynamics.* Molecular Simulation, 1995. **14**(3): p. 137-151.
105. Metropolis, N., et al., *Equation of State Calculations by Fast Computing Machines.* The Journal of Chemical Physics, 1953. **21**(6): p. 1087-1092.
106. Steinbach, P.J. and B.R. Brooks, *New spherical-cutoff methods for long-range forces in macromolecular simulation.* Journal of Computational Chemistry, 1994. **15**(7): p. 667-683.
107. Ewald, P.P., *Die Berechnung optischer und elektrostatischer Gitterpotentiale.* Annalen der Physik (Berlin, Germany), 1921. **369**(3): p. 253-287.
108. Darden, T., D. York, and L. Pedersen, *Particle mesh Ewald: An Nlog(N) method for Ewald sums in large systems.* Journal of Chemical Physics, 1993. **98**(12): p. 10089-10092.
109. Essmann, U., et al., *A smooth particle mesh Ewald method.* Journal of Chemical Physics, 1995. **103**(19): p. 8577-8593.

110. Petersen, H.G., *Accuracy and efficiency of the particle mesh Ewald method.* The Journal of Chemical Physics, 1995. **103**(9): p. 3668-3679.
111. Berendsen, H.J.C., et al., *Molecular dynamics with coupling to an external bath.* Journal of Chemical Physics, 1984. **81**(8): p. 3684-3690.
112. Nosé, S., *A molecular dynamics method for simulations in the canonical ensemble.* Molecular Physics, 1984. **52**(2): p. 255-268.
113. Hoover, W.G., *Canonical Dynamics: Equilibrium Phase-Space Distributions.* Physical Review A: General Physics, 1985. **31**(3): p. 1695-1697.
114. Parrinello, M. and A. Rahman, *Polymorphic transitions in single crystals: A new molecular dynamics method.* Journal of Applied Physics, 1981. **52**(12): p. 7182-7190.
115. Ryckaert, J.-P., G. Ciccotti, and H.J.C. Berendsen, *Numerical integration of the cartesian equations of motion of a system with constraints: molecular dynamics of n-alkanes.* Journal of Computational Physics, 1977. **23**(3): p. 327-341.
116. Hess, B., et al., *LINCS: A linear constraint solver for molecular simulations.* Journal of Computational Chemistry, 1997. **18**(12): p. 1463-1472.
117. Allen, M.P. and D.J. Tildesley, *Computer Simulation of Liquids*. 1987, New York: Oxford University Press.
118. Evans, D.J. and G.P. Morriss, *Statistical Mechanics of Nonequilibrium Liquids*. 1990, London: Academic Press.
119. Evans, D.J. and O.P. Morriss, *Non-Newtonian molecular dynamics.* Computer Physics Reports, 1984. **1**(6): p. 297-343.
120. Hanley, H.J.M., Physica A, 1983. **118**(1).
121. Ciccotti, G. and G. Jacucci, *Direct Computation of Dynamical Response by Molecular Dynamics: The Mobility of a Charged Lennard-Jones Particle.* Physical Review Letters, 1975. **35**(12): p. 789-792.
122. Ciccotti, G., G. Jacucci, and I.R. McDonald, *"Thought-experiments" by molecular dynamics.* Journal of Statistical Physics, 1979. **21**(1): p. 1-22.
123. Heyes, D.M. and J.H.R. Clarke, *Computer simulation of molten-salt interphases. Effect of a rigid boundary and an applied electric field.* Journal of the Chemical Society, Faraday Transactions 2, 1981. **77**(7).
124. Evans, M.W., *Molecular dynamics simulation of induced anisotropy. I. Equilibrium properties.* The Journal of Chemical Physics, 1982. **76**(11): p. 5473-5479.
125. Evans, M.W., *Molecular dynamics simulation of liquid anisotropy. II. Rise and fall transients on a picosecond time scale.* The Journal of Chemical Physics, 1982. **76**(11): p. 5480-5483.
126. Evans, M.W., *Computer simulation of liquid anisotropy. III. Dispersion of the induced birefringence with a strong alternating field.* The Journal of Chemical Physics, 1982. **77**(9): p. 4632-4635.
127. Evans, M.W., *Computer simulation of liquid anisotropy. IV. Terms to second order in the external field of force.* The Journal of Chemical Physics, 1983. **78**(9): p. 5403-5407.
128. Evans, M.W., *Computer simulation of liquid anisotropy. V. Nonlinear molecular dynamics at high field strengths.* The Journal of Chemical Physics, 1983. **78**(2): p. 925-930.
129. Evans, W.A.B. and J.G. Powles, *The computer simulation of the dielectric properties of polar liquids. The dielectric constant and relaxation of liquid hydrogen chloride.* Molecular Physics, 2006. **45**(3): p. 695-707.
130. Zhu, S.B., J. Lee, and G.W. Robinson, *Molecular-dynamics study of nonpolar molecular liquids in intense laser fields.* Physical Review A, 1988. **38**(11): p. 5810-5816.
131. Zhu, S.B., J. Lee, and G.W. Robinson, *Effects of an intense picosecond laser on liquid carbon disulfide: a molecular dynamics study.* Journal of the Optical Society of America B, 1989. **6**(2).
132. Zhu, S.B., J.B. Zhu, and G.W. Robinson, *Molecular-dynamics study of liquid water in strong laser fields.* Physical Review A, 1991. **44**(4): p. 2602-2608.
133. Ohkubo, J., et al., *Molecular alignment in a liquid induced by a nonresonant laser field: Molecular dynamics simulation.* J Chem Phys, 2004. **120**(19): p. 9123-32.

134. Tang, Y.W., I. Szalai, and K.-Y. Chan, *Non-equilibrium molecular dynamics simulation study of the frequency dependent conductivity of a primitive model electrolyte in a nanopore.* Molecular Physics, 2002. **100**(10): p. 1497-1505.
135. Petravic, J. and J. Delhommelle, *Conductivity of molten sodium chloride in an alternating electric field.* The Journal of Chemical Physics, 2003. **119**(16): p. 8511-8518.
136. Evans, M.W., *Molecular dynamics computer simulation of magnetisation by an electromagnetic field.* Physics Letters A, 1991. **157**(6-7): p. 383-390.
137. English, N.J. and J.M. MacElroy, *Theoretical studies of the kinetics of methane hydrate crystallization in external electromagnetic fields.* J Chem Phys, 2004. **120**(21): p. 10247-56.
138. Humphrey, W., A. Dalke, and K. Schulten, *VMD: Visual molecular dynamics.* Journal of Molecular Graphics, 1996. **14**(1): p. 33-38.
139. Starzyk, A. and M. Cieplak, *Proteins in the electric field near the surface of mica.* Journal of Chemical Physics, 2013. **139**(4): p. 045102.
140. English, N.J., P. O'Brien, and G.Y. Solomentsev, *Non-equilibrium molecular dynamics study of electric and low-frequency microwave fields on hen egg white lysozyme.* Abstracts of Papers of the American Chemical Society, 2009. **238**.
141. Lugli, F., et al., *Electric Field Effects on Short Fibrils of A beta Amyloid Peptides.* Journal of Chemical Theory and Computation, 2010. **6**(11): p. 3516-3526.
142. Nelson, R. and D. Eisenberg, *Recent atomic models of amyloid fibril structure.* Current Opinion in Structural Biology, 2006. **16**(2): p. 260-265.
143. Arendash, G.W., et al., *Electromagnetic field treatment protects against and reverses cognitive impairment in Alzheimer's disease mice.* Journal of Alzheimer's disease, 2010. **19**(1): p. 191-210.
144. Hung, A., et al., *Effects of oxidation, pH and lipids on amyloidogenic peptide structure: implications for fibril formation?* European Biophysics Journal, 2008. **38**(1): p. 99-110.
145. Shao, J., et al., *Clustering molecular dynamics trajectories: 1. Characterizing the performance of different clustering algorithms.* Journal of Chemical Theory and Computation, 2007. **3**(6): p. 2312-2334.
146. Solomentsev, G.Y., N.J. English, and D.A. Mooney, *Effects of external electromagnetic fields on the conformational sampling of a short alanine peptide.* Journal of Computational Chemistry, 2012. **33**(9): p. 917-923.
147. Budi, A., et al., *Comparison of embedded atom method potentials for small aluminium cluster simulations.* Journal of Physics: Condensed Matter, 2009. **21**(14): p. 144206.
148. Astrakas, L., C. Gousias, and M. Tzaphlidou, *Electric field effects on chignolin conformation.* Journal of Applied Physics, 2011. **109**(9): p. 094702.
149. Astrakas, L.G., C. Gousias, and M. Tzaphlidou, *Structural destabilization of chignolin under the influence of oscillating electric fields.* Journal of Applied Physics, 2012. **111**(7): p. 074702.
150. Daura, X., et al., *Peptide Folding: When Simulation Meets Experiment.* Angewandte Chemie International Edition, 1999. **38**(1-2): p. 236-240.